8-2021

Modeling and Evaluation of Utility-Scale Microgrid Investment for Distribution System Planning

Ian Schomer
ischomer@vols.utk.edu

To the Graduate Council:

I am submitting herewith a thesis written by Ian Schomer entitled "Modeling and Evaluation of Utility-Scale Microgrid Investment for Distribution System Planning." I have examined the final electronic copy of this thesis for form and content and recommend that it be accepted in partial fulfillment of the requirements for the degree of Master of Science, with a major in Electrical Engineering.

Fangxing Li, Major Professor

We have read this thesis and recommend its acceptance:

Fangxing Li, Leon M. Tolbert, Hector A. Pulgar

Accepted for the Council:
Dixie L. Thompson

Vice Provost and Dean of the Graduate School

(Original signatures are on file with official student records.)

Modeling and Evaluation of Utility-Scale Microgrid Investment for Distribution System Planning

A Thesis Presented for the
Master of Science
Degree
The University of Tennessee, Knoxville

Ian Schomer
August 2021

DEDICATION

To my parents, Terry and Kathy Schomer; my friends, particularly the Buller-Youngs and Videlas; and my wife Sarah for their unfaltering love and support.

ACKNOWLEDGEMENTS

I would like to thank my major professor, Dr. Fangxing "Fran" Li, for sharing his knowledge and ideas throughout my graduate study, and for being my advocate to enrich my education with additional opportunities. I would also like to thank my research advisor Ben Ollis from Oak Ridge National Laboratory (ORNL) for his close guidance and flexibility, particularly in response to the unexpected changes resulting from the COVID-19 pandemic.

I would like to thank Dr. Hantao Cui for serving as my mentor and teaching me skills that advanced the quality of my research. I am also grateful for my research group colleagues—Haoyuan Sun, Evan McKee, Mariana Kamel, Xiaofei Wang, Dr. Qingxin Shi, Dr. Yan Du, among others—for the way that they made themselves available to me to share their ideas and offer advice.

I would also like to thank Dr. Rafael Castro and the rest of Newton Energy Group (NEG) for providing me with cloud-based computing resources to accelerate my research.

Lastly, I would like to thank the National Science Foundation (NSF) and the Center for Ultra-Wide-Area Resilient Electric Energy Transition Networks (CURENT) for providing me with excellent resources and funding opportunities for my graduate studies.

ABSTRACT

The electrical distribution network faces two great challenges for the immediate future. First, increased affordability of distributed energy resources (DERs)—and advancing control technologies of inverters that interface them to the grid—have driven a shift from a passive to an active distribution network (ADN), which heightens the complexity of system management. Second, the increased frequency of severe weather events and increased potential for a cybersecurity attack necessitate the need for a resilient infrastructure that can respond adaptively to shutdowns within the system. Microgrids (MGs) present a promising framework both to provide hierarchal control of DERs and to increase resiliency with grid-forming and grid-restoring functionality. Though much work has been done to validate the role of MGs in the distribution system, grid owners and utilities need effective methodologies to incorporate MGs into existing system planning frameworks to ensure that this technology is quickly and wisely adopted.

This thesis develops a two-stage optimization framework that models utility investment in medium-voltage microgrids (MVMGs) with consideration to normal and high-stress operating conditions. The problem is designed as a mixed-integer second-order-cone program (MISOCP) compatible with commercial solvers to obtain a global solution. The first stage models MG boundary selection as a multi-area power system splitting problem, co-optimizing network topology along with DER siting and sizing that results in optimal placement of MGs capable of prolonged self-sustainment. The second stage iterates through possible grid reconnection points for each MG to find the optimal point of common coupling (PCC) and optimizes islanding decisions for critical hours.

The proposed two-stage framework was optimized and tested on the IEEE 33-Bus System for baseline, one-area, and two-area cases to analyze and compare the capabilities of the method.

The results of the first case study confirm that including MGs in the planning process can lead to heightened resilience against high-stress events that lead to economic savings. The second case study analyzes the value of islanding in a system planning context and classifies scenarios that could provide additional value streams to justify microgrid investment. Finally, suggestions to foster the continued improvement of utility microgrid planning are discussed in the conclusion.

TABLE OF CONTENTS

LIST OF TABLES

LIST OF FIGURES

CHAPTER 1
INTRODUCTION

1.1 Background

The electric grid is the backbone of the modern, digitized life. The standard of living in the United States is defined with the underlying assumption of a constant and unending supply of power. Its value is especially apparent with COVID-19 emerging around the time of this work; the presence of the electric grid in combination with digital technology and the internet has enabled much of the world to work and operate from home, thus sustaining many business sectors and preventing a complete economic crash.

In its conventional architecture, electric power is produced in large quantities at generation plants often located far from load centers. A transmission network carries this power at high voltage for reduced losses to substations near concentrated load centers, where the power is stepped down in voltage and distributed to industrial, commercial, and residential customers. This system architecture is largely one-directional and passive on the distribution side, where a centralized authority handles its operation and management.

In recent decades this legacy architecture has experienced changes outside the scope of its original design due to the adoption of more renewable energy technology, credited to a combination of codependent factors. The need for renewable energy has been extensively quantified by research evidencing the negative environmental impacts of carbon-based emissions

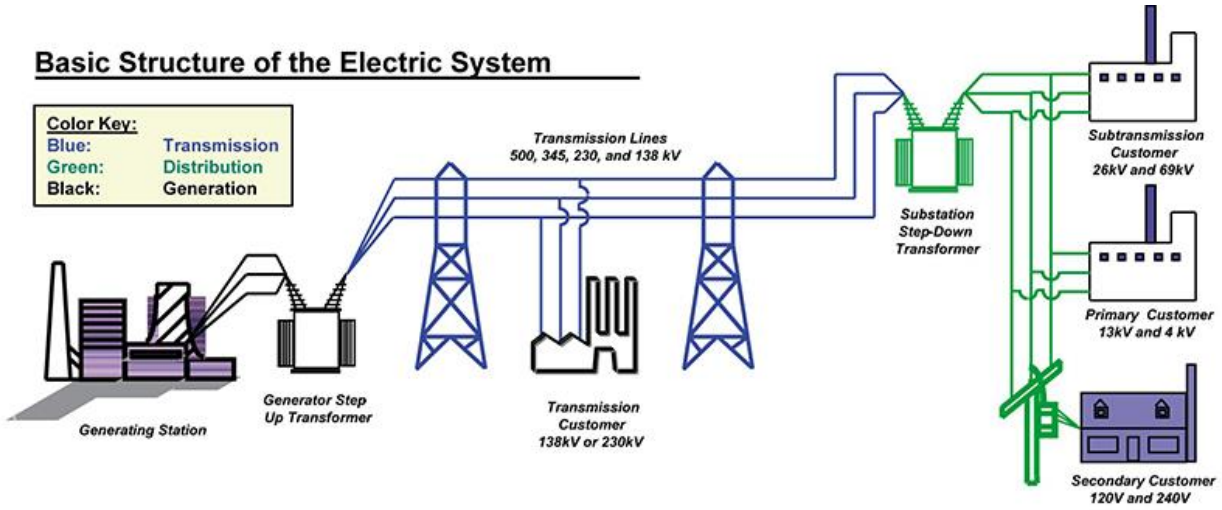

Figure 1: Traditional grid structure, where power flows unidirectionally from right to left (licensed under CC BY-NC)

released from human drivers such as fossil fuel-based generators [4]. Moreover, the economic costs of renewable energy have continued to plummet over the past decade, rendering them cost competitive (and in some applications, undeniably cheaper) compared to fossil fuel-based generation [5]. Thus, on the distribution side in particular, a shift has occurred from a "passive" to an "active" distribution network (ADN) as utilities invest in large-scale renewables, customers integrate more modular distributed energy resources (DERs) behind-the-meter, and information and communication technology (ICT) continues to increase in its capability to connect the two [6].

DERs include distributed generators (DGs)—both conventional and renewable technologies—as well as energy storage (ES). Over the past decades, renewable energy sources as a subset of DGs have continued to increase in its penetration into the grid network. Coupled with increasing inverter capabilities and smart control architectures, renewable DGs have the capability to support local frequency and voltage as well as provide other ancillary services to the grid in ways that conventional generation never could [7]. However, with new technology comes new operational challenges. For instance, renewable resource availability schedules (e.g. a daily sunlight irradiance curve) are not aligned with the daily aggregate load curve, which can lead to reverse power flows and voltage rise upstream during times of overgeneration [8]. Moreover, consumer investment in DERs creates a new category of market participant—the "prosumer"—whose decisions affect the operating state of the grid and thus increase its complexity to manage [9].

If managed properly, integration of DERs and flexible loads can be a great boon to the day-to-day operations of the distribution network and can even provide additional value streams that were not previously accessible. Traditionally, the distribution system was managed solely by the distribution system operator (DSO), which receives remote monitoring data and sends out control

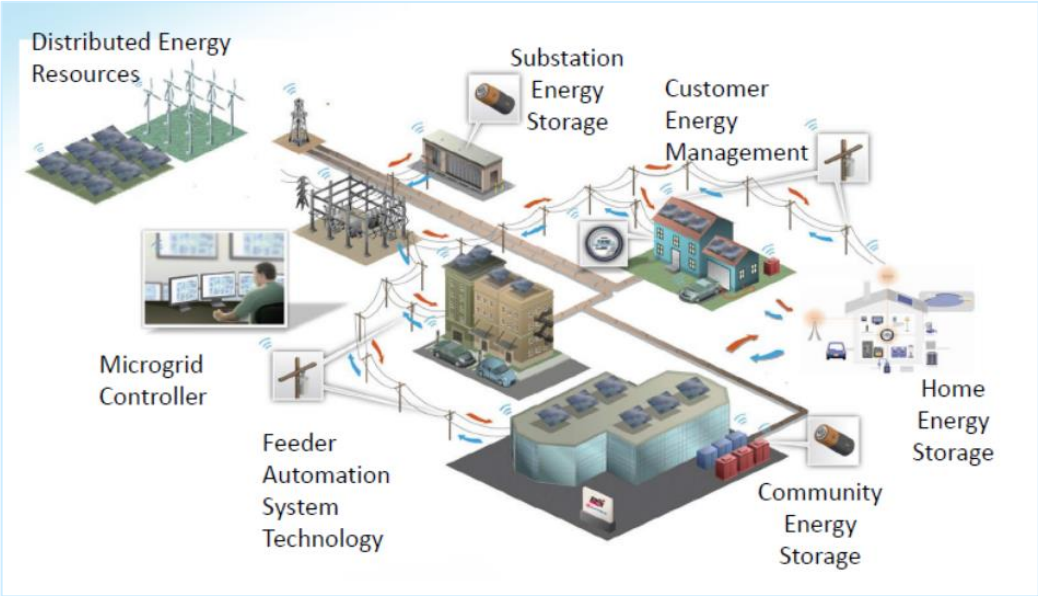

Figure 2: ADN components, including DERs and MG (licensed under CC BY-SA-NC)

signals to equipment in the field. Within the past two decades, the microgrid concept has been developed to shift part or all of this management role away from a centralized entity and allow for meaningful two-way communication. A microgrid (MG) is defined as a controllable collection of DERs equipped with two-way communication channels and connected to the distribution grid solely at the point of common coupling (PCC) [10]. A salient characteristic of a microgrid is its ability to operate in either grid-connected or islanded mode, which contributes to a system by reducing critical load shedding and enhancing black start capabilities [11].

For these reasons, the way that future systems are planned—and existing systems upgraded—should incorporate these active components as part of the decision-making process. This is often the role of the local utility company. Since the traditional distribution system was designed to be radial and passive, planning for future increases in system load meant upgrading substation and equipment capacities to withstand the magnitude of power forecasted to flow through them [12]. Now there exist new opportunities to defer these expensive upgrades by installing DERs to meet demand locally, thereby reducing branch flows and the losses that result [13]. Moreover, the role of the microgrid—or even networks of microgrids—in distribution system planning (DSP) is largely unexplored at the present time. Adding to the challenge of the problem is the fact that metrics such as deferment value are nontrivial to quantify and are subject to interpretation. Nonetheless, the role of DERs and microgrids in the DSP problem remains an active and exciting field of research.

1.2 Literature Review

Expansive research on new ways to perform DSP have created a foundation of modeling techniques from which this thesis was built and has expanded. The first of these major categories is DG siting and sizing. In its broadest form, DG siting and sizing is the problem class of finding the optimal locations and capacity ratings of DGs to enhance a future system [14]. The literature for this topic is quite abundant and mature, with numerous optimization techniques applied and various considerations added. Most works form mixed-integer linear or convex models for global optimization with future system cost as the primary objective [15-17]. The need for binary decision variables arises from the discrete decision of whether to install some DER technology at a given location. Notable additions to this classic framework are the consideration of environmental concerns such as operating constraints [16] and the consideration of investment timing [18], where the latter work frames the problem using real option analysis via a least square Monte Carlo method to model stochastic variables over time.

Another major addition to the planning problem is the consideration of topology changes to the network (either the addition of new lines or the reconfiguration of existing ones) for greater efficiency. Modeling network reconfiguration (NR) introduces additional binary variables and can create nonconvexities, especially when modeling AC power flow. For this reason, some works simplify the power flow model to form a mixed-integer linear program (MILP) that is very efficient to solve [19]. However, sacrifices to the accuracy of a model can lead to inherent suboptimality or potential infeasibility of the global solution with consideration to the actual system being modeled. For this reason, the authors of [20] and [21] propose convex representations of NR that employ conic relaxations of the AC power flow that retains much better accuracy. Since that time, numerous works have been able to achieve global co-optimization of DER investment and NR

while modeling AC power flow. For instance, [22] solves optimal long-term DG investment and NR over different planning stages, and [23] finds an optimal ES allocation with hourly reconfiguration using inverter-based soft open points (SOPs) in place of tie switches for added control. It should be noted that, for traditional switching equipment, hourly reconfiguration should be avoided because frequent operation causes wear and tear on the equipment that outweighs any incremental gains in efficiency.

The third major category is the development of microgrid planning studies. The diversity of literature around this topic reflects the fact that MGs can be considered from a multitude of perspectives relative to level of isolation, internal vs. external system modeling, and ownership. Since a core function of a MG is sustained operation in islanded mode, one subset of this field focuses solely on planning a microgrid to sustain loads in remote areas without an external grid connection [24, 25]. For grid-connected MGs, many works focus on the optimal resource investment, configuration, and scheduling of the microgrid itself, where the external network is reduced to an infinite bus to model power exchanges [26-30]. Notably, some works also optimize network topology, e.g. through a variant of particle swarm optimization (PSO) [31] or with multi-agent reinforcement learning [32]. These methods are similar in that they can model complex interactions abstractly with computational efficiency but cannot guarantee a global solution.

In general, the research described above that focuses on the internals of the MG best represents situations where the MG investor is not concerned with the operation of the power system. In the case where utility investment in MGs is specifically considered—as it is in this thesis—it is often desirable to focus instead on the primary distribution network when considering a MG's potential benefits for DSP. The study in [33] solves for optimal location of low-voltage microgrids (LVMGs) within a primary distribution system using an improved binary genetic

algorithm (IBGA). However, each LVMG is rendered as a one-bus model since the secondary distribution level is not modeled, so it is consequently reduced to a single controllable load from the utility perspective. Utility investment in larger medium-voltage microgrids (MVMGs) have a greater potential for added resilience and economic savings in the primary distribution network, which would naturally be of greater concern to the utility.

This problem class of MVMG formation is particularly interesting because it is modeled not as a single binary decision to install within a network node but as a *partitioning* of the existing network to create the boundaries of the MGs. Most of the research conducted of this type optimizes the formation of one or multiple MVMGs after a fault in the network to minimize unserved load [34-39]. The aforementioned examples borrow principles from graph theory to incorporate concepts such as radiality and connectedness in linear and convex representations.

This thesis seeks to apply modeling techniques similar to those used in post-fault MVMG formations to the context of DSP. A few works have already attempted similar problems [40-42]. The authors of [40] and later [41] propose a two-stage microgrid topology planning process consisting of (1) network splitting based on a traditional graph-partitioning algorithm and (2) integer-based optimization of topology within each partitioned area to create loop-based MGs containing DG and ES. This method relies on a single representation of the load and generation profiles (peak load and nameplate capacity, resp.) to plan the network topology, which does not consider the interactions between seasonal load variation and weather-dependent DER capacity. Moreover, operational bounds based on power flow modeling—a tried-and-true approach for providing assurance of system feasibility—are not addressed or included. The authors of [42] include power flow and voltage modeling in a DER and MG planning framework; however, the approach includes two aspects that limit optimality. First, the problem is split into two separate

optimizations: DG optimal allocation, and a combined MG formation and ES allocation. Second, a dominated group-search optimization (DGSO) method is used for each optimization that solves quickly but, like all meta-heuristic techniques, cannot guarantee an optimal solution and is sensitive to initial states. As will be discussed, this thesis attempts to avoid the aforementioned issues in its solution approach.

1.3 Contributions and Organization

With the relevant literature in mind, this thesis proposes a DSP solution framework for optimal utility investment in MVMGs. The proposed framework consists of two stages. The first stage models fixed-budget DER investment and MG[1] topology planning as a mixed-integer second-order-cone problem (MISOCP) that models AC power flow on historical data to ensure reliable future system operation at least cost. Since second-order cone problems are convex by definition, the first stage is solved by a commercial off-the-shelf solver for a global solution. Fuel-based Conventional Turbines (CT), Photovoltaics (PV), and Lithium-Ion Energy Storage (ES) are included as DER investment options with corresponding operational constraints. The second stage determines the optimal reconnection points and critical islanding decisions for each MG through iteration and reduced MISOCP programming. This stage is designed with the flexibility to be implemented on a different dataset than the first stage in order to evaluate the performance of the planned system over new and larger datasets for increased solution robustness.

[1] This thesis will refer to "MVMG" as "MG" interchangeably hereafter, since the context has already been properly established.

The proposed framework is analyzed for baseline, one-area, and two-area cases and studied in detail. The perspective of the utility is taken by performing economic analysis on the resulting solutions and by providing insights on the available cost metrics. The resilience of the optimal solutions is also analyzed with selected testing data. An in-depth investigation of the value of MG islanding under normal operating conditions is also presented, from which salient findings are offered to improve the quality of future research in this field.

The rest of this thesis is organized as follows. Chapter 2 introduces the various modeling components that were selected, adapted, or proposed that collectively form the MISOCP multi-area optimization model of the first stage. Next, Chapter 3 explains the two-stage utility microgrid investment framework. Chapter 4 delineates the full application of the proposed framework, including the preparation of a test system and historical data as well as two case studies that demonstrate various aspects of its functionality. Lastly, Chapter 5 summarizes the research of this thesis and offers several carefully considered avenues for its future expansion.

CHAPTER 2
MODELING TECHNIQUES FOR DISTRIBUTION FEEDER PLANNING

2.1 Problem Description

The work of this thesis takes on the scope of a medium-voltage DSP problem, where a predicted future load profile requires upgrades to the system in order to ensure feasibility and steady-state stability. The distribution system planner is tasked with determining a solution that minimizes operational costs while satisfying all feasibility requirements. Beyond this basic framework, this thesis explores the co-optimization of several planning decision classes relating to DER and MG capabilities. Three main assumptions were made to narrow this problem class down into one that could be thoroughly explored and analyzed:

1. A fixed expansion budget has been provided to the system planner to be allocated toward DER capital costs.
2. The system planner can alter the states of pre-existing switching equipment to reconfigure the default network topology.
3. The DSO has acquired inverters with advanced control technologies to enable the islanded operation of a subset of the medium-voltage network, including the transitions to and from islanded and grid-connected states.

Thus, the main decision classes of the resulting optimization problem are the following: DER siting and sizing, network line status, and MVMG boundary assignment.

A major goal and accomplishment for this thesis was to synthesize existing modeling techniques into a single framework capable of producing a global solution from a commercial

solver. The methods included below are thus the end result of a process of finding a set of models that could be synthesized without introducing irreducible nonconvexities. The main challenge of this task is rooted in the overlapping levels of binary logic required to model the various planning decisions, each of which project onto the same set of variables representing system states (e.g. voltage and current).

For the following discussion, let Ω_L be the set of lines (both opened and closed) for a given distribution feeder, and Ω_B be the set of all buses within that feeder, where $N_B = |\Omega_B|$ and $N_L = |\Omega_L|$. The set of all reference buses (the substation bus and any MG reference buses) is represented by Ω_{ref}. Buses are assigned to one area from the set of desired areas Ω_A, where $N_A = |\Omega_A|$. The set of all generators in the system is denoted Ω_G, and this includes power from the substation; $\Omega_G(i)$ is the set of generators at bus *i*. In the sections that follow, assume $i \in \Omega_B$, $l \in \Omega_L$, and $a \in \Omega_A$ unless otherwise stated in the equation.

2.2 Optimal Power Flow Model

$$\min \sum_{t=1}^{T} \left[\sum_{i \in \Omega_B, g \in \Omega_G} C_i^g P_{i,t}^g + \sum_{i \in \Omega_B} C_i^{shed} P_{i,t}^{shed} \right] \tag{2.1}$$

s.t.

$$P_{i,t}^{inj} = \sum_{g \in \Omega_G(i)} P_{i,t}^g - \left(P_{i,t}^D - P_{i,t}^{shed} \right) \tag{2.2}$$

$$Q_{i,t}^{inj} = \sum_{g \in \Omega_G(i)} Q_{i,t}^g - \left(Q_{i,t}^D - Q_{i,t}^{shed} \right) \tag{2.3}$$

$$P_{i,t}^{inj} + \sum_{j \in \pi(i)} \left(P_{ij,t}^f - I_{ij,t}^2 r_{ij} \right) - \sum_{j \in \delta(i)} P_{ji,t}^f = 0 \tag{2.4}$$

$$Q_{i,t}^{inj} + \sum_{j \in \pi(i)} \left(Q_{ij,t}^{f} - I_{ij,t}^{2} X_{ij} \right) - \sum_{j \in \delta(i)} Q_{ji,t}^{f} = 0 \tag{2.5}$$

$$V_{j,t}^{2} = V_{i,t}^{2} - 2\left(r_{ij} P_{ij,t}^{f} + x_{ij} Q_{ij,t}^{f} \right) + \left(r_{ij}^{2} + x_{ij}^{2} \right) I_{ij,t}^{2}, \quad \forall i \in fb, j \in tb \tag{2.6}$$

$$\underline{V}_{i} \leq V_{i,t} \leq \bar{V}_{i} \tag{2.7}$$

$$\left(P_{l,t}^{f} \right)^{2} + \left(Q_{l,t}^{f} \right)^{2} = I_{l}^{2} V_{l}^{2} \tag{2.8}$$

Eq. (2.1) – (2.8) describe a basic optimal power flow (OPF) model using the DistFlow method [43], which was originally introduced for radial network reconfiguration applications to model power flow with network losses in a computationally efficient manner. The objective (2.1) is to minimize operation costs consisting of the generation and load shed costs, which are approximated with fixed, first-order cost parameters C. Eq. (2.2) and (2.3) define the dependent injection variables that are used in the power flow constraints. Eq. (2.4) and (2.5) describe the nodal power balance, where $\pi(i)$ and $\delta(i)$ are the upstream parents and downstream children of bus *i*, respectively; (2.6) relates electrically adjacent bus voltages through a voltage drop expression; (2.7) constrains the voltage to ensure stability and to minimize stress on the system components; lastly, (2.8) defines the relationship between real and reactive power, current, and voltage – all of which are decision variables in the optimization problem. Note that (2.8) is a nonlinear, nonconvex relationship that will be handled later in the problem reformulation.

2.3 Linear Approximation of Thermal Limits

$$\left(P_{ij,t}^{f} \right)^{2} + \left(Q_{ij,t}^{f} \right)^{2} \leq \left(S_{ij}^{max} \right)^{2}, \forall i \in fb, j \in tb \tag{2.9}$$

Eq. (2.9) describes the thermal limits of a distribution line in terms of apparent power, represented by the interior of the blue circle in the complex plane of Figure 3. Although it is possible to convert this constraint into a second-order cone constraint, a linear approximation is commonly used in power system modeling that reduces problem complexity with minimal error. Based on the insight that a line flow's real component will almost always be greater than its reactive component in practice, the new feasible region is reduced to the orange shaded area. This area can be approximated by a set of linear inequality constraints, shown in (2.10) – (2.12). This thesis follows convention in the literature (e.g. [23]) by using three lines per flow direction, but more lines can be added to fine tune the tradeoffs between solving time and model accuracy, as explored in [44].

$$-2S_{ij}^{max} \le \sqrt{3}P_{ij,t}^{f} + Q_{ij,t}^{f} \le 2S_{ij}^{max} \tag{2.10}$$

$$-S_{ij}^{max} \le P_{ij,t}^{f} \le S_{ij}^{max} \tag{2.11}$$

$$-2S_{ij}^{max} \le \sqrt{3}P_{ij,t}^{f} - Q_{ij,t}^{f} \le 2S_{ij}^{max}, \quad \forall i \in fb, j \in tb \tag{2.12}$$

2.4 Budget-Constrained DER Siting and Sizing

$$u_i^{CT}\underline{\Gamma}^{CT} \le \bar{P}_i^{CT} \le u_i^{CT}\bar{\Gamma}^{CT}, \forall i \in \Omega_{B\text{å}} \tag{2.13}$$

$$u_i^{PV}\underline{\Gamma}^{PV} \le \bar{P}_i^{PV} \le u_i^{PV}\bar{\Gamma}^{PV}, \forall i \in \Omega_{B\text{å}} \tag{2.14}$$

$$u_i^{ES}\underline{\Gamma}^{ES} \le \bar{P}_i^{ES} \le u_i^{ES}\bar{\Gamma}^{ES}, \forall i \in \Omega_{B\text{å}} \tag{2.15}$$

$$\bar{E}_i^{ES} = h \cdot \bar{P}_i^{ES}, \forall i \in \Omega_{B\text{å}} \tag{2.16}$$

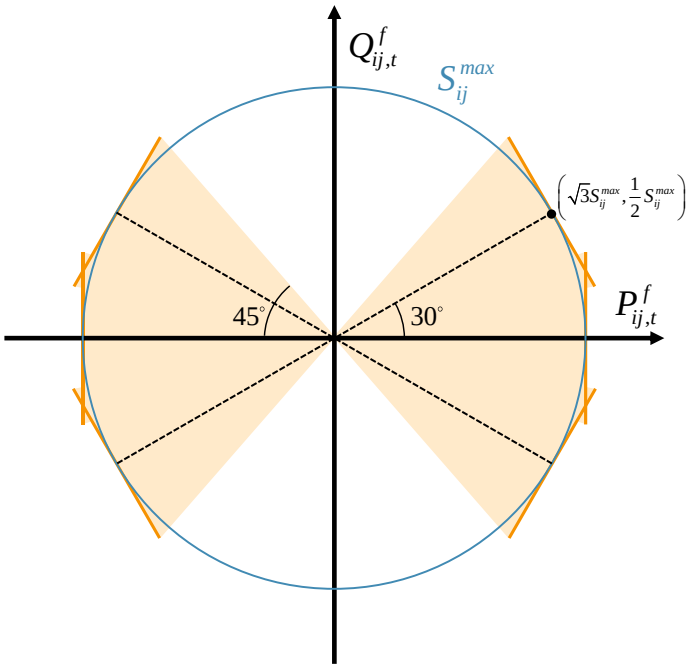

Figure 3: Three-constraint approach to linearize thermal line limits.

$$\sum_{g\in\Omega_G}\sum_{i\in\Omega_{B\text{å}}} \bar{C}_i^{\,g}\bar{P}_i^{g} \le C^{budget} \tag{2.17}$$

This thesis considers CT, PV, and ES as potential DERs to be sited within the distribution system at pre-selected candidate buses $\Omega_{B\text{å}} \subset \Omega_B$. Eq. (2.13) – (2.15) model the siting decision with binary variables *u*: if a DER is not selected for bus *i*, then the installed rating $\bar{P}_i$ for that resource is constrained to zero; otherwise, the rating is constrained to be within a continuous range of realistic size ratings defined by the Γ parameters. For simplicity, we assume a fixed value *h* for the endurance of all ES, i.e., how many hours the battery can sustain its rated power; this relationship is defined by (2.16). Lastly, according to (2.17), the total capital costs (modeled with $/kW unit costs) for all planned installments cannot exceed the given budget.

2.5 Energy Storage Modeling

$$SOC_{\min}\cdot\bar{E}^{ES} \le E_{i,t}^{\ ES} \le SOC_{\max}\cdot\bar{E}^{ES}, \forall i\in\Omega_{B\text{å}} \tag{2.18}$$

$$E_{i,t+1}^{ES} = E_{i,t}^{ES} + \eta_{ch}P_{i,t}^{ch} - \eta_{dis}^{-1}P_{i,t}^{dis}, \forall i\in\Omega_{B\text{å}} \tag{2.19}$$

$$E_{i,1}^{ES} = E_{i,T}^{ES} + \eta_{ch}P_{i,t}^{\ ch} - \eta_{dis}^{-1}P_{i,t}^{\ dis}, \forall i\in\Omega_{B\text{å}} \tag{2.20}$$

$$0 \le P_{i,t}^{\ ch} \le \bar{P}_i^{ES} \tag{2.21}$$

$$0 \le P_{i,t}^{\ dis} \le \bar{P}_i^{ES} \tag{2.22}$$

Eq. (2.18) – (2.22) model the operation of a general energy storage device or system over a continuous time period modeled by discrete decision times $t = 1\ldots T$ (assumed to be hours here). Eq. (2.18) limits the state of charge (SOC) to be within a certain range to promote longevity of the ES. Eq. (2.19) connects the ES's stored energy for the next hour with its current energy level and

its grid-side charging and discharging power $P_{i,t}^{ch/dis}$; losses are modeled with constant charging and discharging efficiencies, denoted η_{ch} and η_{dis}, respectively. Note that E_t^{ES} refers to the amount of energy stored in the ES at time the *beginning* of hour t; hence, Eq. (2.20) is written as such and not as $E_1^{ES} = E_T^{ES}$, as is seen often in the literature. Lastly, Eq. (2.21) and (2.22) limit the grid-side power injection of the ES to its rated power. Note that there is no explicit constraint to dictate that the battery[2] cannot charge and discharge simultaneously. However, this is not necessary, since the non-unity charging and discharging efficiencies guarantee that such a decision would be economically inefficient and therefore suboptimal in the optimization problem.

2.6 Network Reconfiguration and Power System Splitting

This subsection presents an approach adapted from [45] that enables power system splitting via one-time network reconfiguration into N_A radial subnetworks, denoted "areas." It is assumed that a subset of lines $\Omega_{Lå} \subset \Omega_L$ are capable of switching; the other lines are fixed as active in the network. For ease of notation, each line *l* in the network can be described with a "from" bus $f(l)$ and "to" bus $t(l)$ such that $f(l), t(l) \in \Omega_B, \forall l \in \Omega_L$; note that a negative real power flow across any line means that the "to" bus is actually upstream of the "from" bus.

$$\sum_a x_{i,a} = 1, \forall i \in \Omega_B, x_{i,a} \in \{0,1\} \tag{2.23}$$

$$x_{\Omega_{ref},:} = I_{N_A} \tag{2.24}$$

[2] In this work "ES" and "battery" will be used interchangeably, since the ES is assumed to be a Lithium-ion battery for unit cost estimations.

$$\sum_{l} y_l = N_B - N_A, y_l \in \{0,1\} \tag{2.25}$$

Eq. (2.23) describes the fact that each bus can only be assigned to one area, and (2.24) assigns all reference buses to a distinct area using an identity matrix of size N_A. Here the binary variable $x_{i,a}$ denotes whether bus *i* belongs to area *a*. Radiality in the multi-area network is described by (2.25), which is equivalent to constraining the number of lines in each area to be equal to the number of buses in each area minus one [46]. The binary variable y_l represents the status (open/closed) of line *l*. Intuitively for a power system splitting problem, any lines connecting buses in two different areas should be open; this rule can be expressed using a product of binaries over *x*. In order to reformulate this logic linearly, an auxiliary binary variable *z* is introduced below:

$$z_{l,a} \leq x_{f(l),a} \tag{2.26}$$

$$z_{l,a} \leq x_{t(l),a} \tag{2.27}$$

$$z_{l,a} \geq x_{f(l),a} + x_{t(l),a} \tag{2.28}$$

$$y_l \leq \sum_{a} z_{l,a} \tag{2.29}$$

Thus, (2.26) – (2.29) are a mixed-integer linear model of feasible line switching states. Essentially, $z_{l,a}$ is 1 if line *l* belongs internally to area *a*, i.e., if its "from" and "to" buses belong to the same area. Otherwise, the summed expression in (2.29) is equal to zero, and thus the line status is open. Note that (2.29) uses an inequality rather than an equality because there may be more lines than the radiality constraint allows, in which case additional lines internal to an area must be opened.

The radiality constraints presented above, in essence, define the number of lines that should be opened in the system and assign each bus to an area, but it does not explicitly constrain the

solution to be electrically connected within those areas. Thus, there must also be a way to enforce connectivity in each subnetwork to ensure that there exists an electrical path between any two buses assigned to the same area. Methods including spanning tree [21] and single commodity flow (SCF) [47] have been developed for this very purpose. SCF was chosen for this thesis because it introduces no additional integer variables to the optimization problem, whereas the spanning tree approach would introduce $|\Omega_{B\text{å}}|$ integer variables [48]. In short, SCF uses a lossless version of a given network topology, where all the reference nodes act as a source to satisfy all non-reference nodes acting as sinks, each of which draw a single unit (i.e. "commodity") from the system. In this way, only a connected network can satisfy this set of constraints; otherwise, there would exist an island without an upstream source node. The method is delineated below:

$$F_i^{inj} \geq 1, \forall i \in \Omega_{ref} \tag{2.30}$$

$$F_i^{inj} = -1, \forall i \notin \Omega_{ref} \tag{2.31}$$

$$\sum_{j \in \delta(i)} F_{ij}^{f} - \sum_{k \in \pi(i)} F_{ki}^{f} = F_i^{inj} \tag{2.32}$$

$$-M_1 y_l \leq F_l \leq M_1 y_l \tag{2.33}$$

Eq. (2.30) and (2.31) assign all buses as either "sources" or "sinks" in the network according to their reference status. Note that, since any feasible solution to this set of constraints must be an integer, then all new variables introduced in this section can be modeled continuously. The commodity flow is described by (2.32), which is an expression of nodal balance. Lastly, (2.33) relates the SCF to the NR variables by restricting the flow to zero on any opened line, where M_1 is a large constant that effectively removes the constraint for lines that are closed.

2.7 Probability-based Weighting

In general, DSP seeks to determine the best planning decisions to prepare a system for future states. A common approach to model future states in an optimization framework is to select a characteristic set of time intervals (hours for this discussion) that includes a variety of load, weather, and price scenarios. However, in the spirit of finding an economically efficient solution, the question should be raised as to whether each hour should contribute equally to the cost function. If the dataset includes a particularly rare anomaly, for example, it could be argued that an estimate of the long-term operational cost of the system should consider the cost of this hour to a lesser degree than that of other hours, since the risk of such an occurrence is low in comparison.

This thesis incorporates the preceding rationale by assigning a probability-based weight within the objective function to each hour of the dataset. This weight is determined using the cumulative probabilities (i.e. $P(X \geq x)$) of the occurrence of a particular day (24-hour period), relative to a historical dataset, for the following three categories:

1. Severity of *load* (total system real power demand)
2. Severity of *price* (locational marginal price (LMP) from the transmission network)
3. Severity of *weather* (cloudiness/darkness indicated by available PV capacity).

In this way, historical days that are less severe and therefore more typical receive a larger weight in the objective function and thus have more influence on the planning decision. After the weights have been calculated, they can be normalized to provide a more meaningful metric, though it does not affect the optimal solution.

The code written to generate the probabilistic weights is summarized in Algorithm 2.1 below. Note that the probabilities calculated are for each day as a whole, since the ES operational

constraints contain time dependencies on a daily resolution. The daily probabilities can then be projected onto each hour of that day during optimization.

Algorithm 2.1

Select a set of characteristic days $\Omega_{Days} = \{d | d \in [1, 365]\}$;
Select a data sample $S \subset \Omega_{Days}$;
Reshape the historical datasets LMP, k^{PV}, and P^D into 24-h periods such that $LMP(d)$ gives the 24 hourly prices for day d, and so on;
For *s* in *S* **do**
    $\lambda^{LMP} \leftarrow \max LMP(s)$;
    $\lambda^{PV} \leftarrow \sum k^{PV}(s)$;
    $\lambda^{D} \leftarrow \sum P^{D}(s)$;
    $X \leftarrow \{d \mid \max LMP(d) \geq \lambda^{LMP}$ and $\sum k^{PV}(d) \leq \lambda^{PV}$ and $\sum P^{D}(d) \geq \lambda^{D}\}$;
    $\omega(s) = |X|$;
End for
$\omega = \omega \,/\, \sum \omega$;
Return ω

CHAPTER 3
PROPOSED DISTRIBUTION PLANNING FRAMEWORK

3.1 MISOCP Multi-Area System Planning Model

$$\min \sum_{t=1}^{T} \omega_t \left[\sum_{i \in \Omega_B, g \in \Omega_G} C_i^g P_{i,t}^g + \sum_{i \in \Omega_B} C_i^{shed} P_{i,t}^{shed} \right] \tag{3.1}$$

s.t.

(2.2), (2.3), (2.10) – (2.33)

$$P_{i,t}^{inj} + \sum_{j \in \pi(i)} \left(P_{ij,t}^f - w_{ij,t} r_{ij} \right) - \sum_{j \in \delta(i)} P_{ji,t}^f = 0 \tag{3.2}$$

$$Q_{i,t}^{inj} + \sum_{j \in \pi(i)} \left(Q_{ij,t}^f - w_{ij,t} X_{ij} \right) - \sum_{j \in \delta(i)} Q_{ji,t}^f = 0 \tag{3.3}$$

$$\underline{V}_i^2 \le v_{i,t} \le \overline{V}_i^2 \tag{3.4}$$

$$\left\| \begin{array}{c} 2P_{l,t}^f \\ 2Q_{l,t}^f \\ w_{l,t} - v_{l,t} \end{array} \right\|_2 \le w_{l,t} - v_{l,t} \tag{3.5}$$

$$-M_2 \left(1 - y_{ij}\right) \le -v_{j,t} + v_{i,t} - 2\left(r_{ij} P_{ij,t}^f + x_{ij} Q_{ij,t}^f\right) + \left(r_{ij}^2 + x_{ij}^2\right) w_{ij,t} \le M_2 \left(1 - y_{ij}\right), \quad \forall i \in fb, j \in tb \tag{3.6}$$

$$-M_3 \cdot y_l \le P_{l,t}^f \le M_3 \cdot y_l \tag{3.7}$$

$$-M_3 \cdot y_l \le Q_{l,t}^f \le M_3 \cdot y_l \tag{3.8}$$

$$-M_4 \cdot y_l \le w_{l,t} \le M_4 \cdot y_l \tag{3.9}$$

$$\underline{P}_i^{CT} \le P_{i,t}^{CT} \le \overline{P}_i^{CT}, \forall i \in \Omega_{B\text{å}} \tag{3.10}$$

$$0 \le P_{i,t}^{PV} \le k_t^{PV} \bar{P}_i^{PV}, \forall i \in \Omega_{B\text{å}} \tag{3.11}$$

$$-\theta^{CT} \cdot P_{i,t}^{CT} \le Q_{i,t}^{CT} \le \theta^{CT} \cdot P_{i,t}^{CT}, \forall i \in \Omega_{B\text{å}} \tag{3.12}$$

$$-\theta^{PV} \cdot P_{i,t}^{PV} \le Q_{i,t}^{PV} \le \theta^{PV} \cdot P_{i,t}^{PV}, \forall i \in \Omega_{B\text{å}} \tag{3.13}$$

$$0 \le P_{i,t}^{shed} \le \gamma P_{i,t}^{D}, \gamma \in [0,1] \tag{3.14}$$

$$Q_{i,t}^{shed} = \theta^{pq} P_{i,t}^{shed} \tag{3.15}$$

Eq. (3.1) and the proceeding constraints represent the full MISOCP model that constitutes the first stage of the planning framework, and will be referred to hereafter as Model (3.1). The objective function (3.1) incorporates the probability-based weighting method described in Section 2.7. The nonconvex portion of the DistFlow method has been convexified in (3.2) – (3.9), as originally proposed in [20]. Notably, the square of the voltages and currents have been replaced with new variables *v* and *w*, respectively. The P-Q-I-V relationship in (2.8) is first relaxed into an inequality and then transformed into a second-order cone (SOC) constraint, as described in [23] Appendix A. Eq. (3.7) – (3.9) constrain the flow to zero for any opened line; here the Big-M constants (also in (3.6)) preserve linearity while effectively removing the constraint if the line status is set to closed. Eq. (3.10) and (3.11) define generation limits for the CTs and PVs, respectively (power from the substation is unconstrained). Power factor constraints are linearly approximated in (3.12) and (3.13) with the parameter θ, which is related to power factor (PF) by $\theta = \tan\left(\cos^{-1} PF\right)$. Finally, (3.14) and (3.15) ensure that load shedding at bus *i* cannot exceed a set percentage of local demand, and θ^{pq} is implemented to keep the PFs of the nodal demands and load shedding equal.

In short, the solution to Model (3.1) is a set of N_A electrically separated areas optimized for least-cost operation of the collective set. A microgrid, then, is modeled as any area without a

substation bus. This stage of the proposed planning framework optimizes all planning decision variables.

3.2 Post-Planning Optimization of Microgrid Islanding

$$\min (3.1) \tag{3.16}$$

$$s.t.$$

$$(2.2),\ (2.3),\ (2.10) – (2.33)$$

$$(3.2) – (3.5),\ (3.10) – (3.15)$$

$$Y_{l,t}^{isl} = 0, \forall l \notin \Omega_{PCC}, t \notin \Omega_{Isl} \tag{3.17}$$

$$\begin{aligned} -M_2\left(\left(1-y_{ij}\right)+Y_{:,t}^{isl}\right) \le -v_{j,t} + v_{i,t} - 2\left(r_{ij}P_{ij,t}^{f} + x_{ij}Q_{ij,t}^{f}\right) + \left(r_{ij}^2 + x_{ij}^2\right)w_{ij,t} \\ \le M_2\left(\left(1-y_{ij}\right)+Y_{:,t}^{isl}\right), \forall i \in fb, j \in tb \end{aligned} \tag{3.18}$$

$$-M_3 \cdot \left(y_l - Y_{:,t}^{isl}\right) \le P_{l,t}^{f} \le M_3 \cdot \left(y_l - Y_{:,t}^{isl}\right) \tag{3.19}$$

$$-M_3 \cdot \left(y_l - Y_{:,t}^{isl}\right) \le Q_{l,t}^{f} \le M_3 \cdot \left(y_l - Y_{:,t}^{isl}\right) \tag{3.20}$$

$$-M_4 \cdot \left(y_l - Y_{:,t}^{isl}\right) \le w_{l,t} \le M_4 \cdot \left(y_l - Y_{:,t}^{isl}\right) \tag{3.21}$$

In general, it is more economical for MGs that exist in the context of a grid system to operate in grid-connected mode under normal conditions. For this reason, after the MG boundaries are established through the optimization of Model (3.1), a modification of the MISOCP formulation can be solved that reconnects the MGs at their PCCs and models the ability to switch between grid-connected and islanded mode. The system costs obtained from this second optimization provides a more realistic estimate of the long-term operational costs of MG

investments. Moreover, the utilization of a grid-forming inverter within an MG is hypothesized to have the potential to return the MG buses to a safe operating zone when the upstream grid is in a high-stress state (e.g. when high load drives down voltages at the fringes of the grid where the MG resides).

For these reasons, a new binary matrix Y^{Isl} is introduced to model the islanding decision, where $Y^{Isl}_{l,t} = 1$ indicates that a PCC connection at line *l* will disconnect to form an island at time *t*. (Note that the matrix representation is mainly for visual clarity, and only a small subset of binaries within this data structure are represented as independent decision variables after the model reduction process of a commercial solver.) In this way, let $\Omega_{PCC} \subset \Omega_L$ be the set of lines in the network that are assigned as PCC connections after solving Model (3.1), and let Ω_{Isl} be the set of hours for which islanding is to be considered. Thus, (3.17) removes any elements of Y^{isl} as free decision variables that are not associated with a PCC line during an hour of consideration.

Eq. (3.16) is the same objective function as the previous section, but the planning decision variables— $\bar{P}^g, x, y, z$ —are now fixed as constants. Eq. (3.18) – (3.21) add the islanding decision to (3.6) – (3.9), with changes highlighted in blue. Eq. (3.16) and the proceeding constraints will be referred to hereafter as Model (3.16).

3.3 Two-Stage Framework for Optimal Microgrid Planning and Operation

This section provides the complete framework proposed in this thesis to model utility investment in microgrids within a system planning context. The process begins by translating a physical system into the appropriate data structures: Ω_B, Ω_L, etc., and populating all parameters

and constants. From this point onward, Figure 4 outlines the step-by-step process developed that incorporates Models (3.1) and (3.16). The assigned reference buses are the "root" of each electrical area that are formed in the first optimization. After solving Model (3.1), the planner can determine which hours, if not all, to optimize the islanding decision through Ω_{Isl}. Since the topology might allow multiple paths for grid reconnection, the algorithm includes an iterative process to determine the optimal set Ω_{PCC} from all possible sets Ω^{*}_{PCC}. The best solution of Model (3.16) contains the optimal planned system with operational costs that reflect the MG interactions with the upstream network.

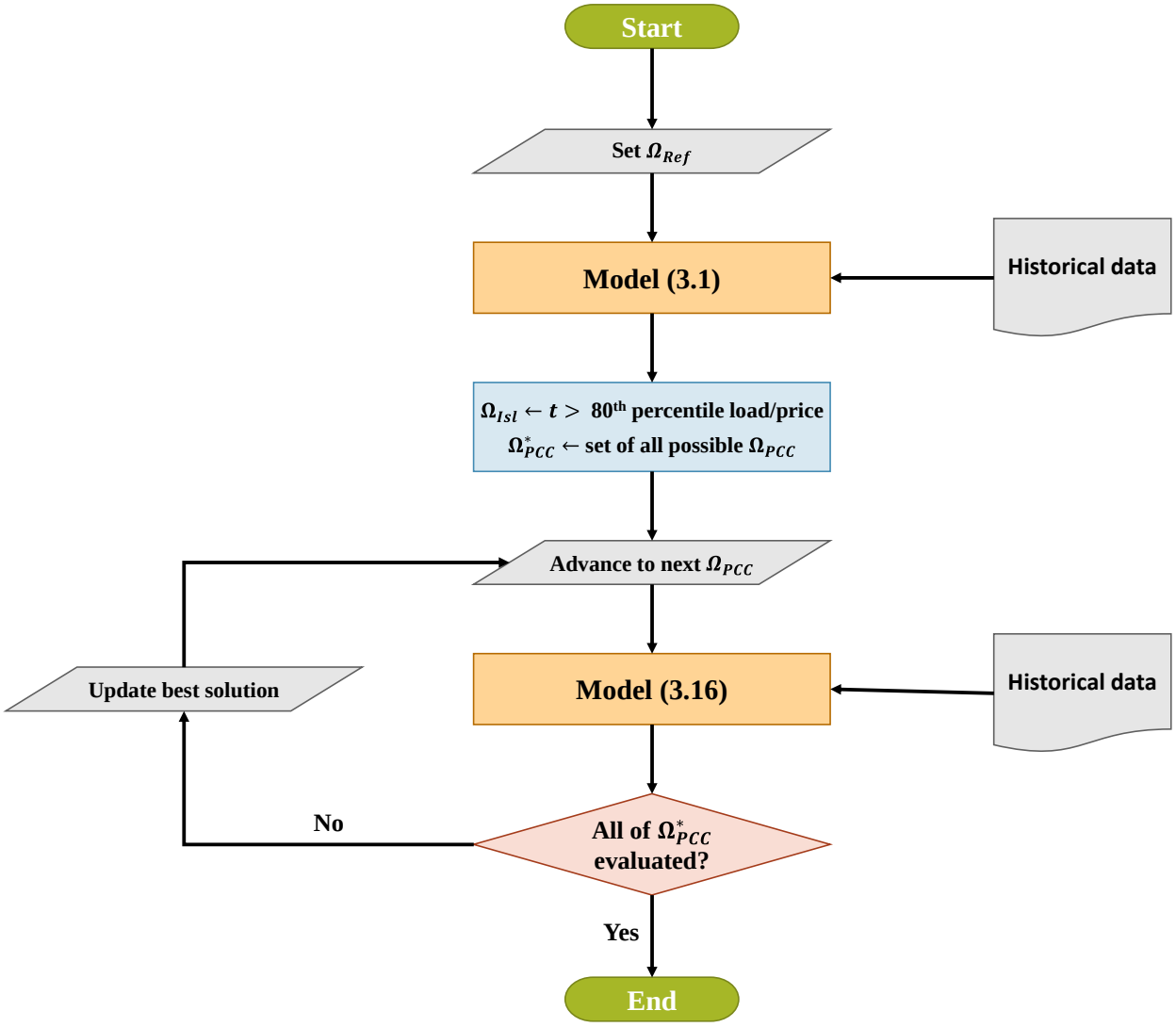

Figure 4: Algorithm schematic for the two-stage optimization framework.

CHAPTER 4
APPLICATIONS AND DISCUSSION

4.1 Test System Description

The 12.66 kV IEEE 33-Bus Feeder was first introduced by [43] to showcase the value of network reconfiguration in distribution systems for reducing losses. Figure 5 shows this system, where node 1 represents the substation bus. The line parameters are unaltered in the following studies, but the load throughout the system is scaled by a constant to model the projected degree of maximum load growth within the planning period. The original system load is 3.75 MW + j2.3 MVar. See the Appendix for a complete list of specifications for the feeder.

The case studies below employ two realistic simplifications to Model (3.1) that increase solver efficiency. First, a subset of all feeder nodes (see $\Omega_{B\text{å}}$ from Section 2.4) is made available to the solver for DER siting, with selected locations based on the intuition that the fringes of the feeder will have lower voltages that are more resilient to times of DER overproduction. Second, a subset of all feeder lines (see $\Omega_{L\text{å}}$ from Section 2.6) is made available for network reconfiguration; this modeling decision dramatically reduces solver time[3] and also reflects the practicality that many lines within a feeder may not have been installed with hardware for reconfiguration. Figure 6 shows the bus and lines selected as planning variables for the following case study. In practice, this method of subset selection would be the responsibility of the distribution planner, who knows the physical system being planned and can make informed decisions that will produce a solution tailored to the characteristics of the feeder.

[3] The line-based binaries are tightly coupled with other variables in the constraints (particularly voltages and line flows, see Eq. (3.6)–(3.9)), which tends to make branch-and-bound algorithms slow to arrive at the global solution.

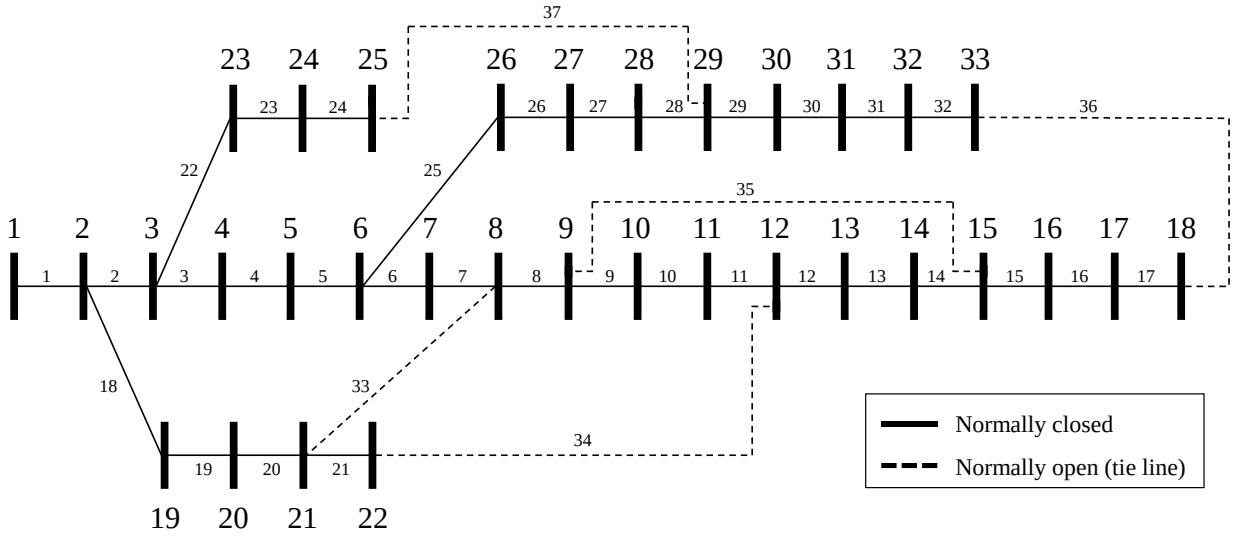

Figure 5: Topology of the IEEE 33-Bus Feeder

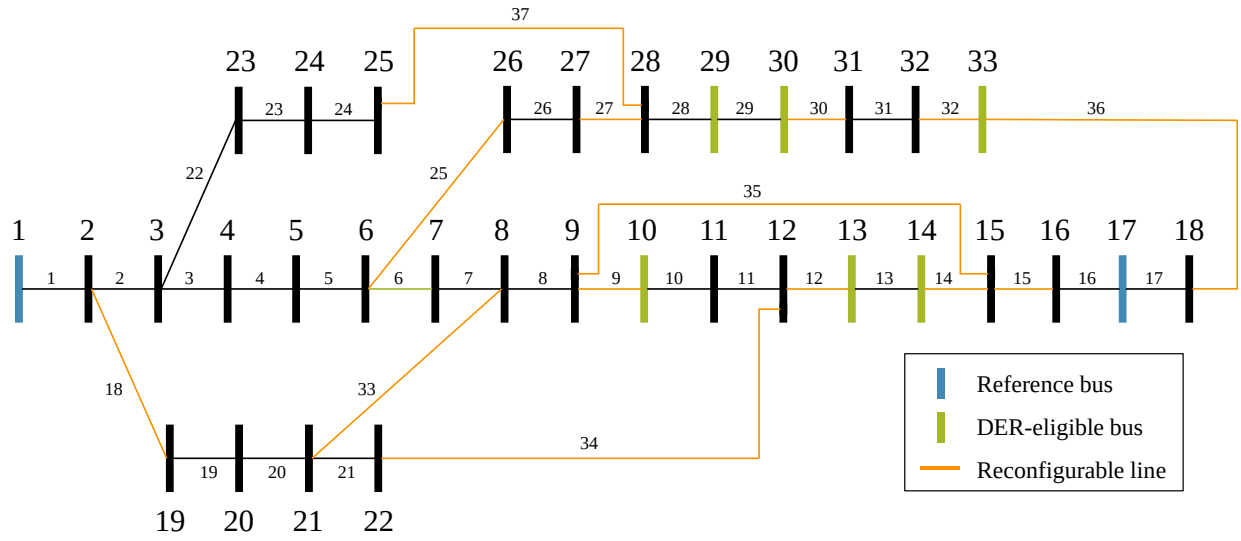

Figure 6: Selection of reconfigurable lines and DER-eligible buses for the IEEE 33-Bus Feeder

4.2 Historical Data Acquisition

As is customary in DSP problems, this thesis employs historical data to generate forecasted profiles of the system load, PV generation capacity, and the LMP at the substation bus. Historical data was extracted through PJM's public archives for the 2019 calendar year using PJM's Data Miner 2 [49]. The time series arrays of PV production and load were normalized so that the profiles could be scaled by the ratings of the PV units and the projected nominal load growth, respectively.

For the case studies described below, the first stage of the planning framework is solved over a set of characteristic days chosen to represent the variation of load shapes, PV capacity curves, and energy prices. This convention highlights the tradeoff between dataset size and power flow model accuracy common to all DSP problems. In this case, a larger dataset is foregone in order to model the intricacies that network reconfiguration decisions have on voltage profiles and line losses within an AC power flow representation.

Analogous to machine learning applications, "overfitting" an optimal solution on a small batch of characteristic data could result in poor performance on new scenarios that are not well represented by the original dataset. For this reason, we introduce another, larger dataset that the first-stage solution is tested on in the second stage to establish a more robust evaluation of performance of the planned system. To be clear, a larger dataset can be incorporated into the second-stage optimization because all binary planning decisions are already optimized in the first stage, so more data can be handled with reasonable solve times. Moreover, the testing dataset can comprise entirely different historical data than the planning dataset because the decisions being optimized are specific to the hour, i.e. economic dispatch and MG operating mode.

Figure 7 displays the load, price, and solar data used for the two stages of the optimization framework. The planning data consists of two typical winter days, two shoulder season days, and

one summer peak day. The testing data comprises four 7-day periods, one for each season, that are meant to capture weekly load patterns as well as give more variety to nodal prices and weather conditions. Note that the first 7-day period includes a winter freeze phenomenon that resulted in very high prices (up to $645.80/MWh) as load surged rapidly in response; this data is meant to test the resilience of the planned systems against future weather uncertainty.

4.3Simulation Environment

The code for the proposed planning framework was written and executed in MATLAB 2019a. YALMIP was integrated to build the constraints and objective function of each subproblem within MATLAB. The optimization models themselves were solved using commercial solvers obtained through academic licenses. Based on best performance, IBM ILOG CPLEX version 12.9 was implemented to solve Model (3.1), and Gurobi version 9.1.1 was used to solve Model (3.16).

An Amazon AWS instance was granted to the author of this thesis via Newton Energy Group (NEG) to run the simulations presented below. The assigned machine was part of a Windows Server 2016 Datacenter running a 64-bit OS with an Intel® Xeon® Platinum 8275CL CPU @ 3.0 GHz and 16 GB RAM.

4.4Case Study I: Method Comparison

Experimental Setup

In the first application, a scenario is proposed where a distribution planner wishes to upgrade an existing system for future load growth on a fixed budget, which could represent the

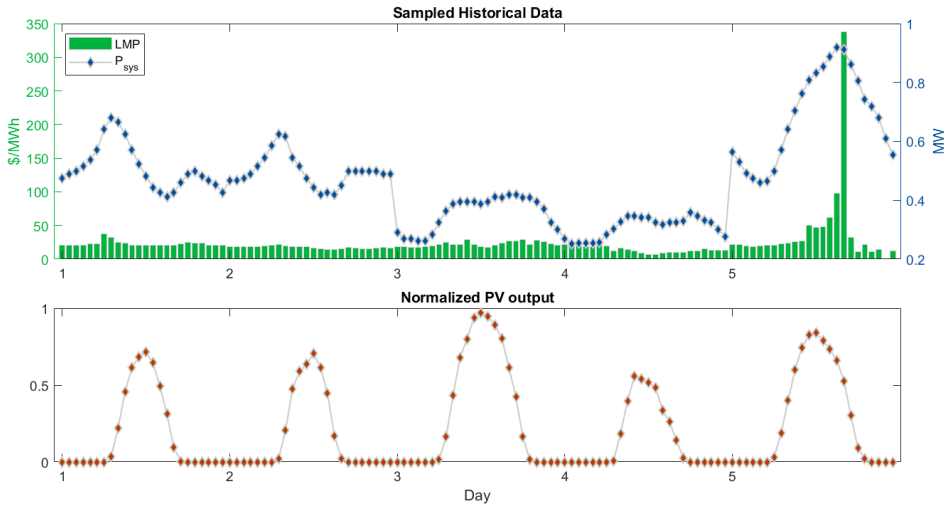

(a)

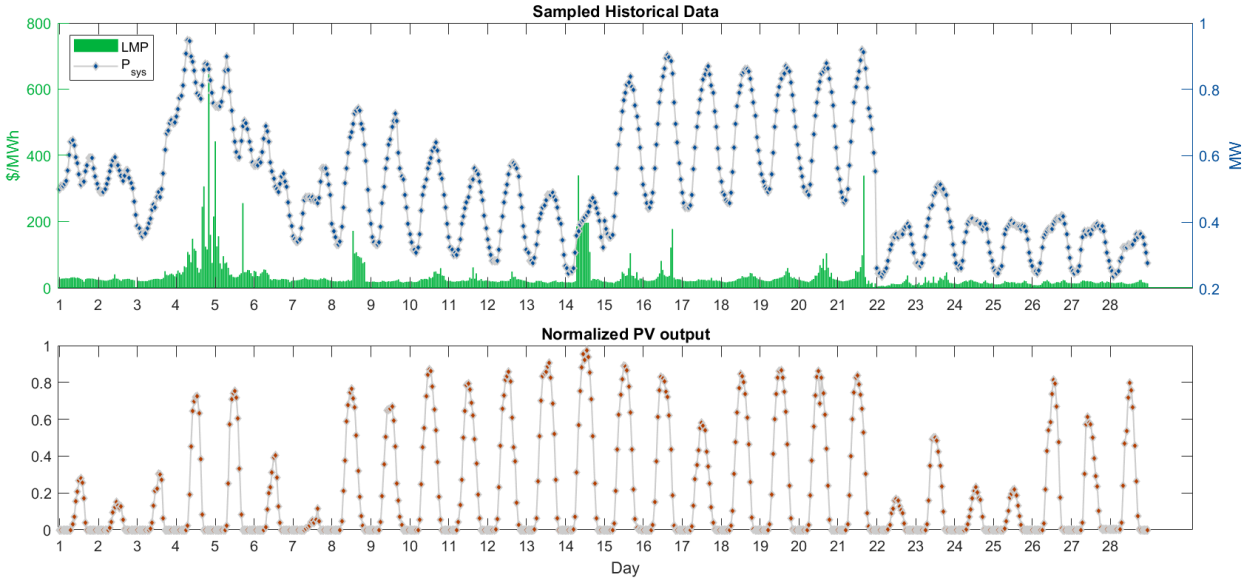

(b)

Figure 7: Load, prices, and PV output profiles (a) for optimizing (first stage) and (b) for testing (second stage)

cost of a traditional wires-based expansion solution. The focus of experimentation was on a two-area solution (such that one microgrid was planned) and was tested against a baseline method, which only optimizes DER siting and sizing. A one-area optimization was also incorporated for testing as a trivial case of Model (3.1), which essentially adds network reconfiguration to the baseline method. These distinctions are summarized in Table 1.

Before proceeding, it should be noted here that the two-area method is not the same optimization problem as the baseline and one-area methods with added degrees of freedom. If this were the case, then the two-area solution would always be trivially more optimal in comparison to the other two (in which case in-depth analysis would have limited value). Instead, the two-area method incorporates the full two-stage optimization framework summarized in Figure 4, whereas the baseline and one-area methods solve Model (3.1) only, since there is no microgrid present to optimize further. Thus, the proceeding analysis evaluates the entire model for MG investment. Also note, however, that the one-area method will always be more optimal than the baseline method because the fixed topology of the baseline method represents one of many feasible topology choices for the one-area method.

To begin the optimization process, the planner selects candidate buses and lines as shown previously in Figure 6. The planner also sets the values of optimization parameters based on knowledge about the physical system, its limitations, and projected load growth over the planning period. In lieu of this knowledge, salient parameters have been set as constant over the following simulations and are listed in Table 2, based on public data and convention in the literature. For simplicity, line flow limits and allowable voltage ranges were held constant over all lines and all

Table 1: Optimization method functionality comparison

Method Name	DER Siting & Sizing	Line Reconfiguration	Microgrid Siting
Baseline	✓		
One-Area	✓	✓	
Two-Area	✓	✓	✓

Table 2: Parameters for the distribution planning problem

Parameter	Symbol	Value	Source
Load Scaler	---	1.5	
Reference buses	Ω_{Ref}	1, 17	
Budget	C^{budget}	$ 4M	
CT Installment Cost	$\bar{C}_i^{CT}$	$ 1,150 / kW	[1]
PV Installment Cost	$\bar{C}_i^{PV}$	$ 850 / kW	[2]
ES Installment Cost	$\bar{C}_i^{ES}$	$ 280 / kWh	[3]
CT Operational Cost	$\bar{C}_i^{CT}$	$ 41 / MWh	[1]
PV Operational Cost	$\bar{C}_i^{PV}$	$ 0 / MWh	
ES Operational Cost	$\bar{C}_i^{ES}$	$ 0 / Mwh	
ES Capacity	$\bar{E}_i^{ES}$	4-hour	[3]
Charge/discharge efficiency	η^{ch}, η^{dis}	0.9, 0.9	
Allowable SOC	SOC_{min} SOC_{max}	[0.4, 1.0]	
CT minimum installment	$\underline{\Gamma}^{CT}$	25 kW	
PV minimum installment	$\underline{\Gamma}^{PV}$	50 kW	
ES minimum installment	$\underline{\Gamma}^{ES}$	50 kW	
Line capacity	S_{ij}^{max}	5 MVA	
Allowable voltage	$\underline{V}_i, \bar{V}_i$	[0.9, 1.05]	
PF limit for CT and PV	θ^{CT}, θ^{PV}	± 0.85	
Max load shed ratio	γ	0.6	

buses, respectively, but the design of the optimization problem does allow for bus-specific and line-specific limits.

Before analyzing the solutions, we begin with a base-case run to determine how the feeder would perform if no planning decisions were made. These results were obtained by running a full one-area optimization with the following modifications: the budget was set to zero; the voltage and line flow constraints were relaxed to large numbers; and the line status was constrained to match the original topology. Looking at Figure 8, the voltage profile of the unplanned system is above the 0.95 p.u. constraint most of the time. From this information the planner could conclude that the forecasted load growth is not large enough to cause a steady-state voltage stability concern after distributed generation is added. The line flows, however, surpass the rated limit for a significant amount of time that necessitates capital investment in the system. Specifically, Lines 1 and 2 exceed the flow limit about 22.5% and 15% of testing hours, respectively. For this reason, it is clear that a capacity expansion or deferment plan is needed to ensure reliable operation of the feeder for the forecasted horizon. Any solution presented hereafter will satisfy these limits over all hours because the framework incorporates them as explicit inequality constraints.

Results Analysis

We begin analysis by visualizing the optimal topologies for the one-area and two-area solutions (the baseline solution shares the same topology as Figure 5). As shown in Figure 9, the one-area solution opened lines 9, 14, 27, and 32 to be replaced with tie lines 34 through 37. Given that these tie lines have comparatively higher impedances, the fact that many of them are found in the optimal solution is quite unintuitive; however, it is important to remember that line losses are proportional to the impedance and the *square* of the current. Thus, using higher-impedance lines

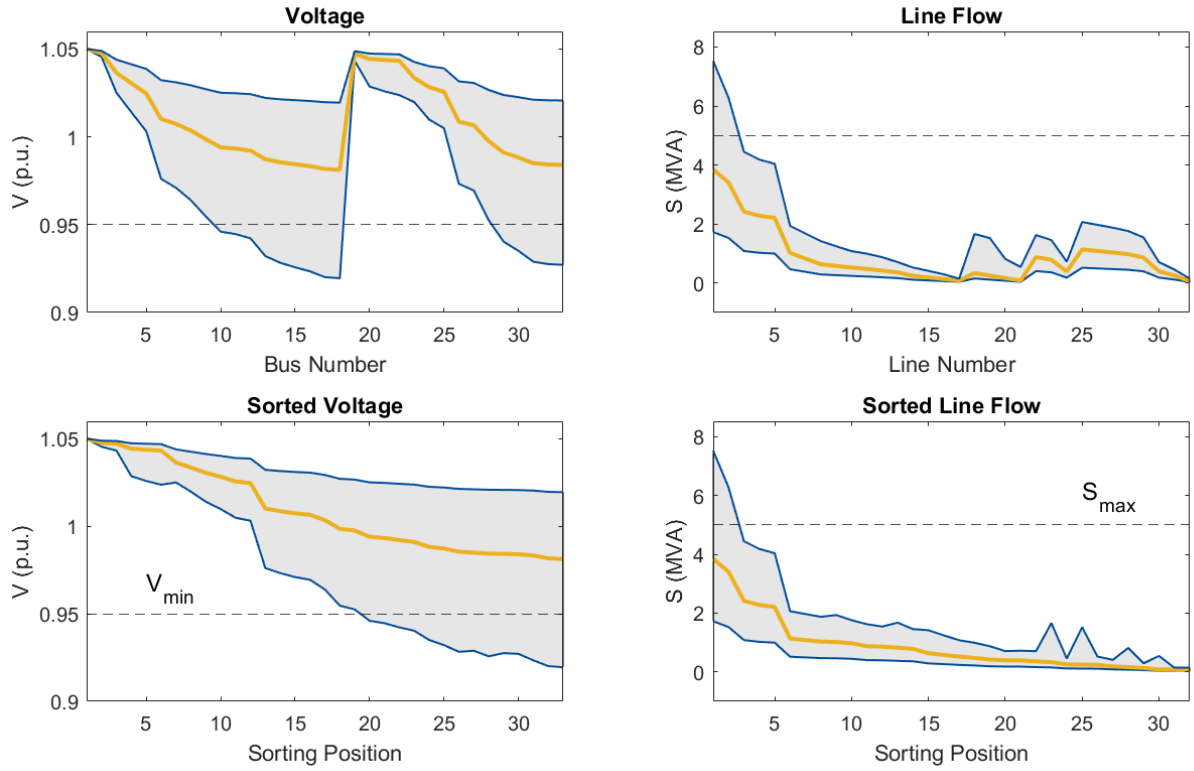

Figure 8: Voltages and line flows (min, mean, max) of the unplanned feeder over the testing data

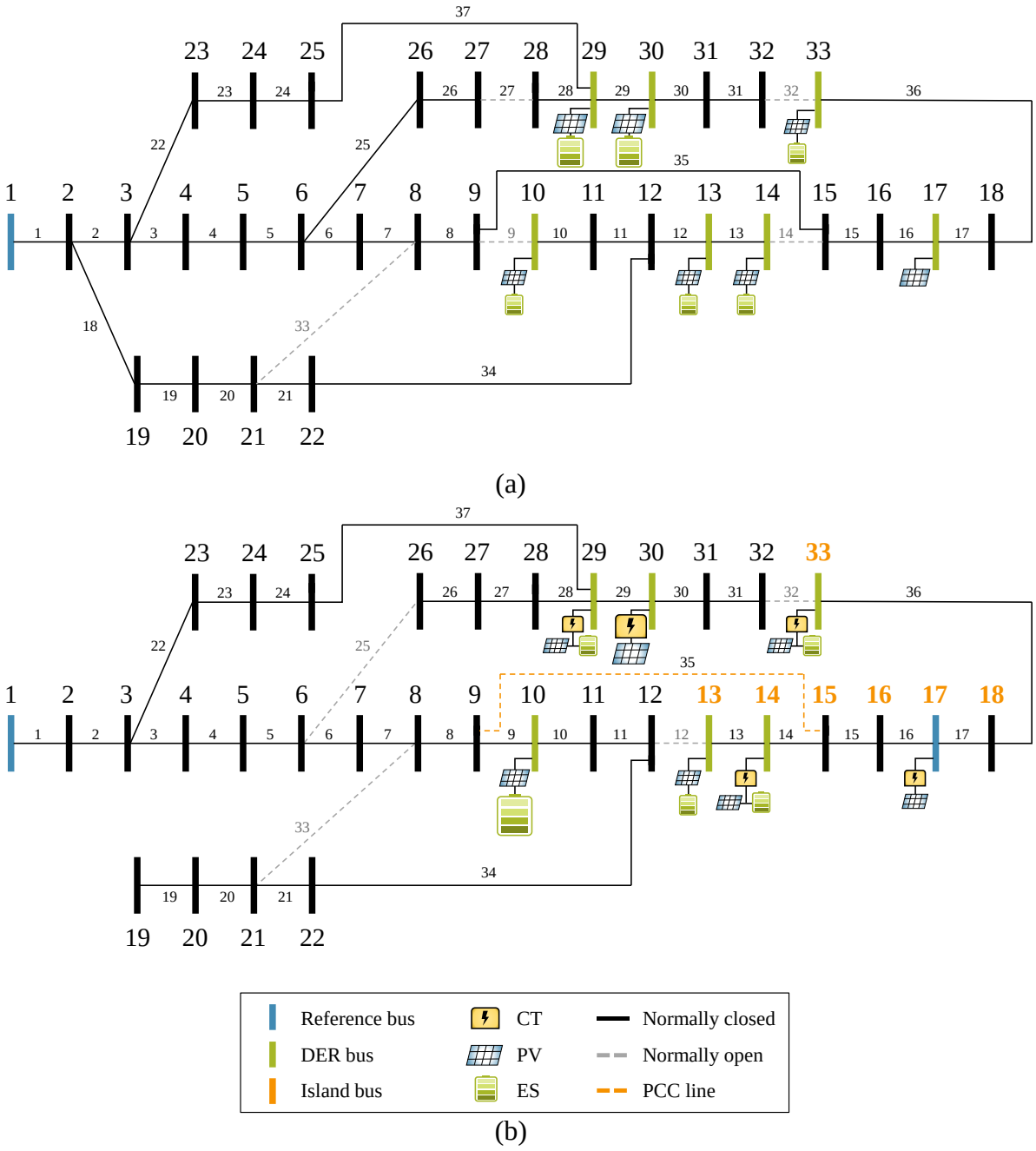

Figure 9: Optimal topologies for (a) one-area and (b) two-area cases; DER icon sizes indicate salient differences.

to achieve a more even distribution of line currents will result in lower line losses. Moving to the two-area method, this solution selected buses 13–18 and 33 to form the island in the first stage, and tie line 35 was chosen in the second stage to act as the PCC. Note that three lines could have been selected as the PCC (12, 32, and 35), but 35 was optimal primarily because this connection most evenly distributes load across the branches and brings the islandable buses closest to the root node in terms of network distance. Interestingly, the optimal topology of the two-area solution effectively reduced the number of branches coming off of the primary feeder (from 3 to 2).

With respect to DER siting, all three solutions used every node made available to it for siting at least one type of resource, and no one resource was sited at its max allowed rating at any of these nodes. This observation suggests that there is value in the modularity of DERs as opposed to a large generation unit at a single point in the network. Another interesting observation is that the largest ES installment for the two-area case was outside of the MG. Since this area receives a time varying LMP signal, the ES at bus 10 is able to add value to the system via energy arbitrage (charging during low prices and discharging during high prices). In contrast, the batteries within the MG were likely sited to help even out the intermittency of PV.

Figure 10 shows the optimal resource procurement mix for the three methods. Since PV is the cheapest DER in terms of unit cost, the baseline and one-area solutions were able to site more capacity than the two-area solution with the same budget. Since the DER locations and capacities are determined in the first stage of optimization, the island must meet load over all characteristic hours without being electrically connected to the substation. For this reason, CTs are sited within the island buses to provide a consistent foundation of generating capacity that can be tapped into when solar resources are insufficient. Since CT is the only DER implemented in this thesis that

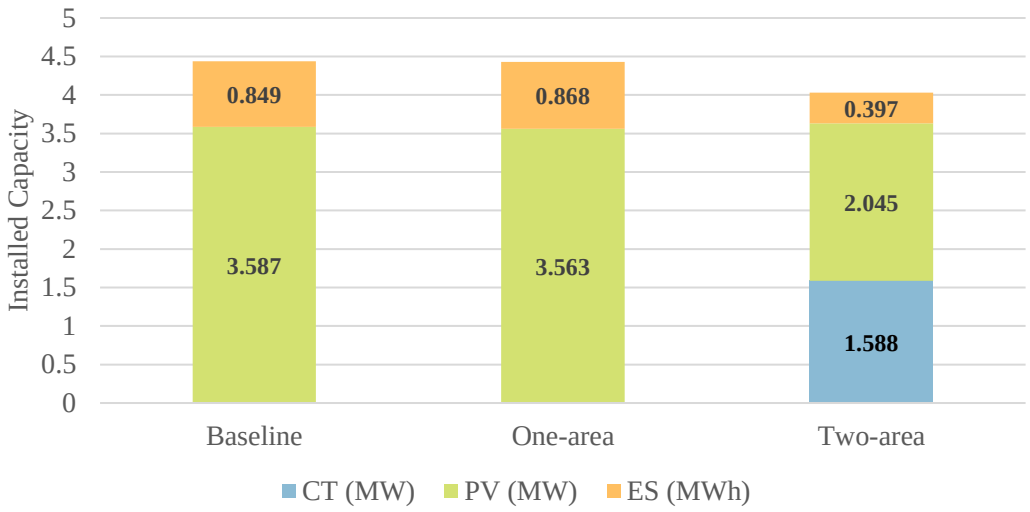

Figure 10: Planned resource mix of the three solutions

has a cost term present in the objective function, it can be concluded that siting more storage within the island instead of CTs was probably infeasible due to its high unit cost under a fixed budget.

Next, voltage profiles were analyzed for each planned system over the testing data in order to gain insight on the effects of network reconfiguration with and without island selection. As all three solutions were given the same budget and same candidate buses for DER siting and sizing, the differences below reflect the effect of topology changes on voltage profiles, which in turn provide insights into the system in two main ways. First, the magnitude of voltage drop *across a line* is proportional to the magnitude of line losses (recall that (2.6) describes voltage drop in terms of line impedance and flow). Second, the magnitude of voltage drop *along a feeder* indicates to what degree the system can maintain steady-state voltages to avoid a potential collapse. Two figures are presented for this reason. Figure 11 displays the magnitude of voltage drop by plotting its cumulative sum over the lines of the system, sorted by descending voltage drop for visual clarity. Figure 12 shows voltage profiles across system nodes ordered by nominal bus number and also by a sorted order from greatest to lowest mean voltage.

Comparing the one-area solution with the baseline solution in Figure 12, it is clear that network reconfiguration results in less voltage drop between adjacent nodes and thus a tighter voltage profile along the edges of the feeder. Note that this tendency for network reconfiguration to benefit system voltages is not specifically prescribed in the objective function but rather is a result of using appropriate cost metrics to drive operational objectives. In this case, selecting a topology that minimized line losses meant that less energy was dissipated and therefore less energy was required to be purchased.

Turning to the two-area solution, we find that the voltage profile is comparable to that of the baseline and lower on average to that of the one-area method, as displayed in Figure 12. The

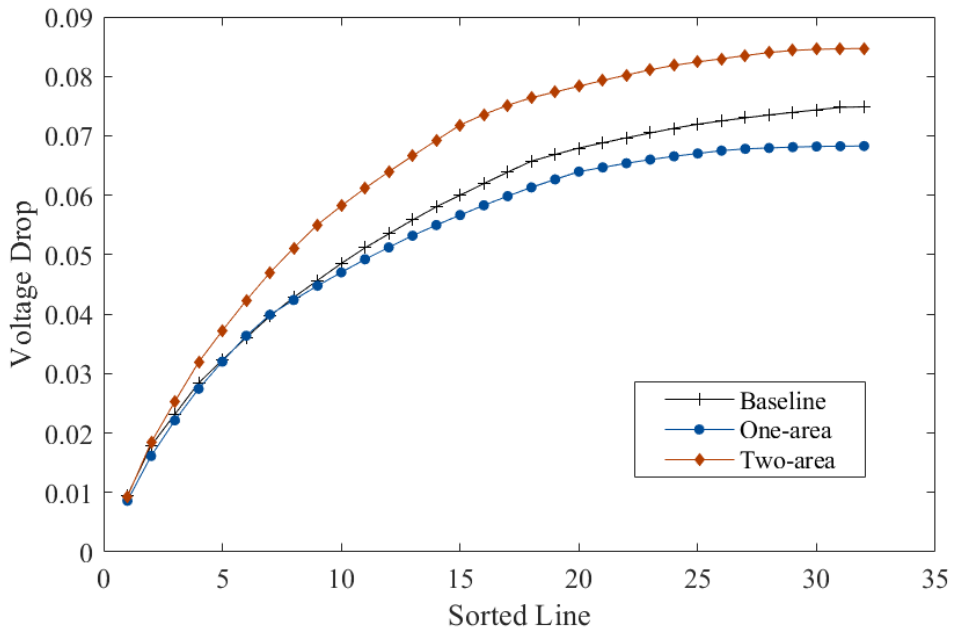

Figure 11: Comparison of cumulative voltage drop (average for each line) across the nodes of the test system.

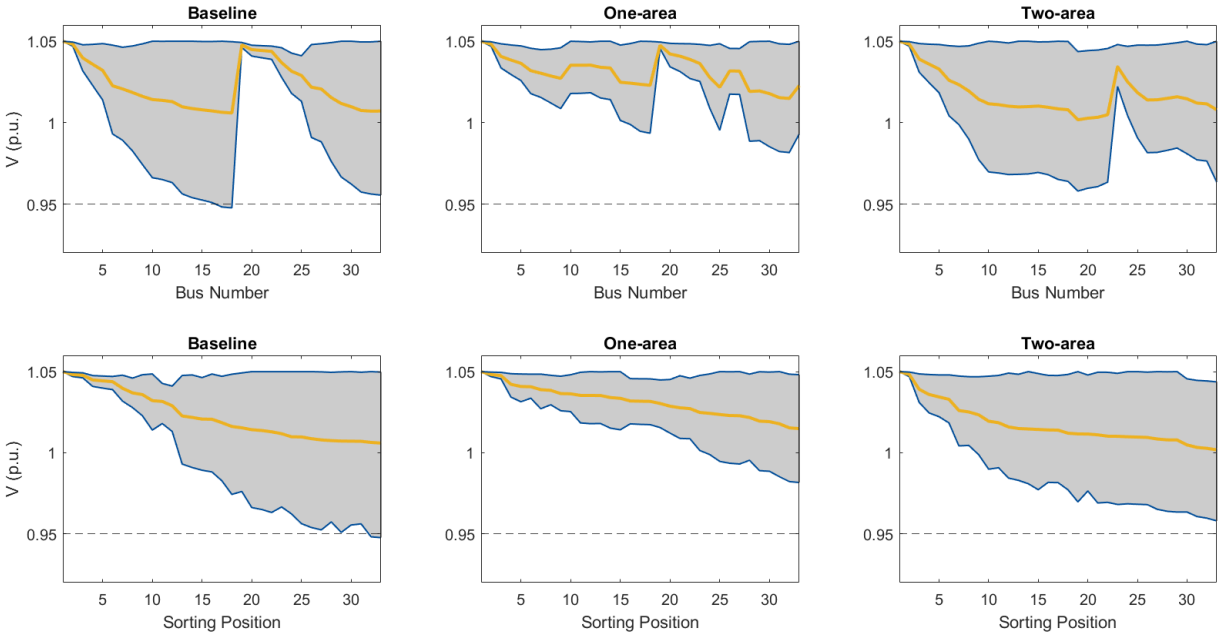

Figure 12: Nodal voltage statistics (min, mean, max) of the optimal solutions over the testing data

network configurations from Figure 9 provide helpful insight to explain this observation. The one-area solution essentially results in a 3-branch topology whereas the two-area solution results in a 2-branch topology. Hence, the length of each branch is longer for the two-area solution in grid-connected mode, so there is a wider voltage range across each branch. Figure 11 indicates that the two-area solution had the highest total voltage drop across the system, on average. The reason for this is a result of the multi-stage process required for convex islanding optimization. Although network reconfiguration was modeled in the same way for both the one-area and two-area methods, the addition of the power system splitting component within the two-area method required any feasible topology to include an electrically separated microgrid. Thus, the economic drivers that influence topology selection were also separated between the two areas without consideration of a grid-connected state. During the testing stage when the microgrid could reconnect to the rest of the system, the feeder branch that received the microgrid buses grew in length and thus was prone to lower voltages.

As a whole, it can be concluded that the optimality for the two-area method in this case study tends toward a utilization of the entire allowable voltage range. Evidently, the increased voltage drop across the system of the optimal state presented here allows for other opportunities to lower costs, most likely related to the positioning of the sited DERs in relation to the rest of the network.

Lastly, the overall annualized system costs were calculated based on the total generation by resource type and load shedding, and are summarized in Table 3. Two metrics are provided in the table that measure performance in different ways. The “weighted production cost” is calculated by determining the probability-weighted average hourly cost over the testing data (as described in Section 2.7), and then performing a scaled sum to obtain a yearly estimate. This quantity essentially

Table 3: Annualized cost comparison of the three solutions

Method	Weighted Production Cost	Raw Production Cost
Baseline	$ 680,130	$ 976,820
One-Area	$ **615,760**	$ 880,530
Two-Area	$ 623,440	$ **777,960**

provides an estimate of future system costs assuming that the total historical dataset provides a good representation of future states. In contrast, the "raw production cost" does not include probability weighting and is simply an annualization of the production cost over the testing data. The raw cost indicates performance on the testing data itself, and note that this could be a better planning metric if historical data is concluded to be a poor representation of future data, e.g. as climate change continues to increase the frequency of severe weather events. Both costs include the cost of load shedding in the calculation of average hourly cost.

Discussion

Looking at the results, the one-area solution is the most economical in terms of weighted production costs, and the two-area solution fares the best over the testing data. The distinction is mainly a result of the sited resource mix. The one-area solution sited more renewable generation capacity, which offset power purchase costs from the transmission network under normal operating conditions. The two-area solution, however, sited more fuel-based generation capacity, which provided more resiliency against load shedding and protected against high transmission prices when renewables were unavailable. Truly, there can be no clear "winner" when considering the tradeoff between robustness and economic efficiency. As with any form of insurance, there is a cost associated with protecting against risk; determining whether this cost is worth paying depends on the likelihood and magnitude of the perceived risk. In this application, the distribution system planner would be tasked with determining which metric from Table 3 more adequately aligns with characteristics of that particular system.

In order to dive deeper into the overall cost, the *cumulative* raw cost was plotted in Figure 13 to highlight the hours which have the largest influence on the total cost. Based on the shape of

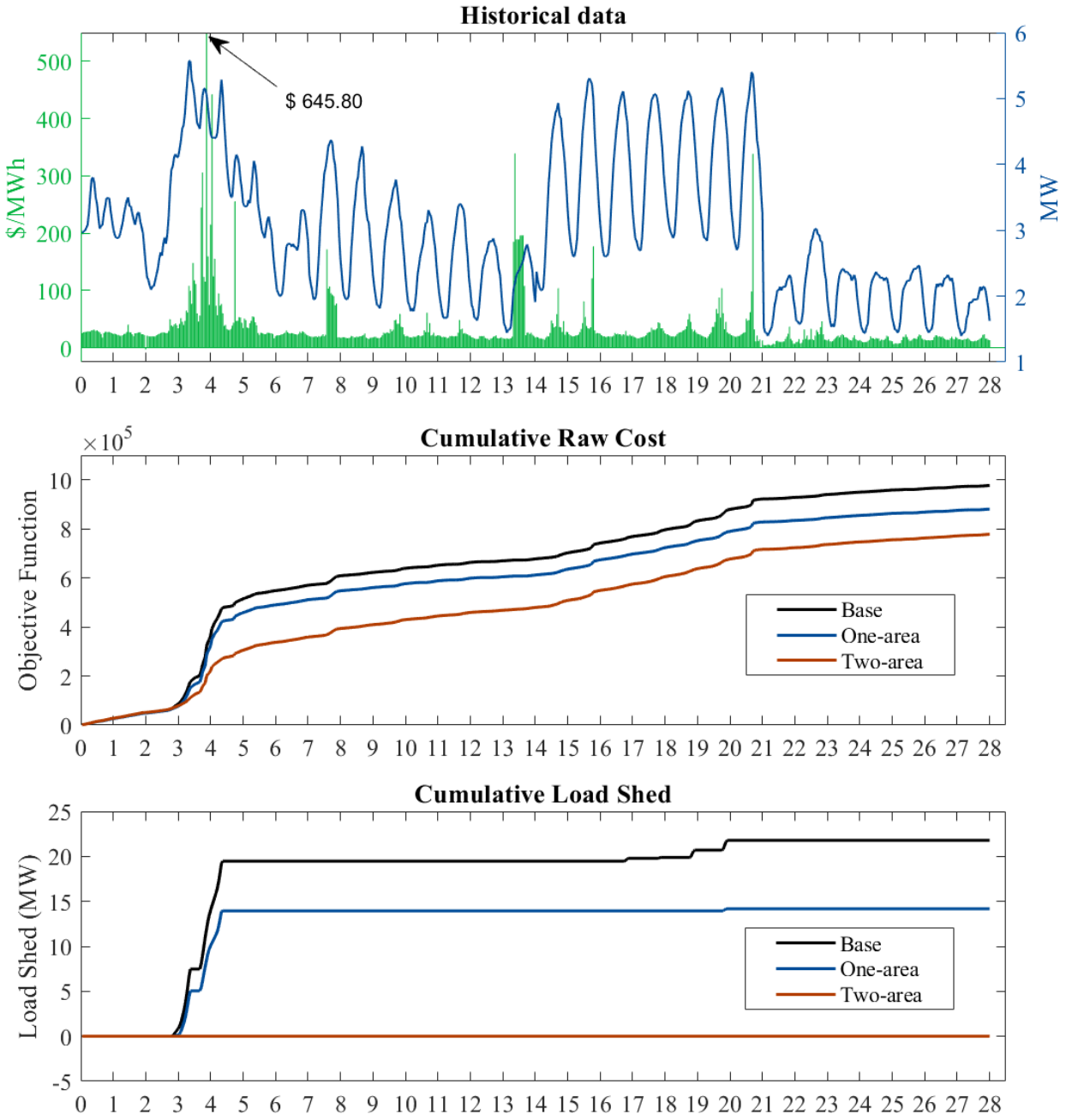

Figure 13: Cumulative raw cost and load shedding measured over the testing data

the curves, it is clear that a few short hours of extreme conditions can be as costly for a power system as a week or more of normal conditions. In this case study, both high load and high prices occur at the end of day 4 after the sun had gone down. Since the voltage constraints were not active across the testing data, it follows that the flow limit going out from the substation bus had reached its limit and required load shedding to maintain safe operation. The two-area solution saved a significant amount of load shedding costs during these hours because it was the only solution to site CTs, which engaged to prevent load shedding. The only other notable period of load shedding occurred within the baseline solution during the high load trends of the representative summer week. The optimal reconfigurations of the non-baseline methods resulted in the avoidance of significant load shedding during these high-load hours.

The shape of the cumulative cost metrics following the extreme conditions of days 4 and 5 were largely equivalent. It was expected that the two-area solution would form its island during high-price hours (e.g. the spike on day 21) that would result in a noticeable reduction of costs. Upon closer analysis of the output, however, it was revealed that the two-area solution did not engage its island for any hour of the testing simulation. Analysis was conducted to investigate why islanding was a suboptimal choice across the testing data; these conclusions will be discussed in the following case study.

4.5 Case Study II: Analysis of Islanding Operation

Experimental Setup

In order to isolate and analyze the processes that define the economics of islanding, a second case study is presented that simplifies some of the modeling techniques of Case Study I.

Most notably, ES was removed as a decision variable to eliminate any temporally coupled constraints that would otherwise influence the decision to island. To illustrate the reasoning behind this decision, consider how the optimal power injection of any resource for Model (3.1), aside from direct generation limits, is mainly dependent on the load, price, and irradiance conditions *for that hour only*, since temporal constraints such as ramping limits are not considered in this thesis. In contrast, the optimal SOC of any sited ES for some hour is dependent on the SOCs of all other hours in that 24-hour period due to constraints (2.19) and (2.20). For this reason, the decision to island for a particular hour of the day could make feasible another SOC profile that is more economical. Thus, ES was removed for Case Study II because this incentive for islanding is more closely related to the interactions of distinct modeling techniques than to the physical effects of islanding that the proposed framework is modeling.

Aside from the removal of ES, all other changes from the parameters shown in Table 2 were made to isolate the conditions where islanding was hypothesized to provide system benefit, as mentioned in Section 3.2. These changes are as follows:

- the line flow constraint was removed to eliminate this type of load shedding;
- the budget was reduced to shift more of the generation to the root node, thereby increasing voltage drop;
- the load scaler was increased when testing for higher line losses, and thus larger voltage drop.

The full list of parameters for Case Study II is shown in Table 4, with changes highlighted in blue.

Results Analysis

As with the previous case study, the parameters listed in Table 4 were fed into the algorithm summarized in Figure 4 to obtain the optimal two-area solution. Figure 14 presents the optimal siting decisions and network configuration of the two-area solution. The result is largely similar to the previous study but with two notable distinctions. First, bus 33 was not assigned to the island during the two-area optimization. Second, the PCC line has shifted to line 36. The optimal investment mix of the network totaled to a nameplate value of about 3.23 MW, as shown in Figure 15; thus, the budget reduction and removal of ES resulted in 800 kW of reduced DER capacity.

The two-area solution of Case Study II again remained grid-connected across the entire testing window.

To understand better the reasons for suboptimality of islanding, a close-up view of the modeled system is presented for two hours of the testing window. The hour $t = 80$ is part of the winter cold snap segment of the testing data; at this time, the sun had set but load and energy price surged, and a small amount of load shedding was required to maintain operational constraints. In contrast, the hour $t = 122$ occurs at the tail end of the extreme conditions, where load had decreased significantly but LMP was still high enough to justify sustaining the operation of the CTs. Table 5 provides a quantitative comparison of the two hours being analyzed.

Figure 16 presents a visualization of (1) the line flow directions around the PCC line and (2) the voltage profile starting from the root node and moving in network order to the end of the branch containing the island. The grey box within the voltage charts indicates the buses shown in the network diagrams. Starting with $t = 80$, all DERs are injecting at their maximum allowable capacities. The flow directions indicate that all sited DER locations except bus 13 have excess

Table 4: Parameters for the second case study

Parameter	**Symbol**	**Value** (optimizing → testing)
Load Scaler	---	1.5 → **2.5**
Reference Buses	Ω_{Ref}	1, 17
Budget	C^{budget}	**$ 3.5M**
CT Installment Cost	$\bar{C}_i^{CT}$	$ 1,150 / kW
PV Installment Cost	$\bar{C}_i^{PV}$	$ 850 / kW
ES Installment Cost	$\bar{C}_i^{ES}$	---
CT Operational Cost	$\bar{C}_i^{CT}$	$ 41 / MWh
PV Operational Cost	$\bar{C}_i^{PV}$	$ 0 / MWh
ES Operational Cost	$\bar{C}_i^{ES}$	---
ES Capacity	$\bar{E}_i^{ES}$	---
Charge/discharge efficiency	η^{ch}, η^{dis}	---
Allowable SOC	SOC_{min} SOC_{max}	---
CT minimum installment	$\underline{\Gamma}^{CT}$	25 kW
PV minimum installment	$\underline{\Gamma}^{PV}$	50 kW
ES minimum installment	$\underline{\Gamma}^{ES}$	---
Line capacity	S_{ij}^{max}	---
Allowable voltage	$\underline{V}_i, \bar{V}_i$	$[0.95, 1.05]$
PF limit for CT and PV	θ^{CT}, θ^{PV}	± 0.85
Max load shed ratio	γ	0.6

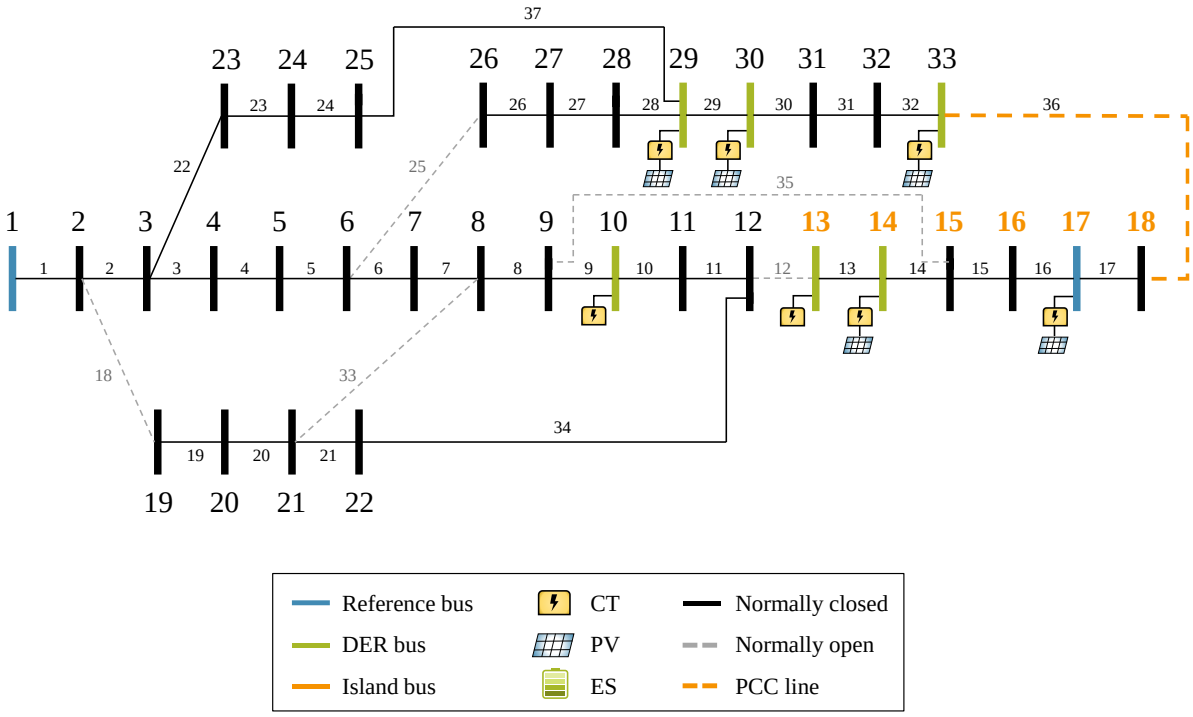

Figure 14: Two-area optimal topology for Case Study II.

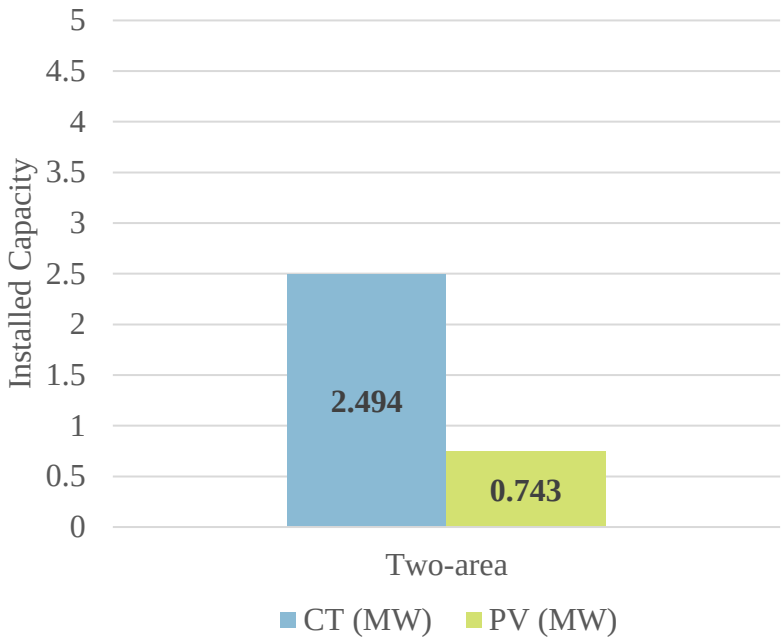

Figure 15: Resource investment mix for the solution of Case Study II.

Table 5: Comparison of the 80th and 122nd hours of the testing data

	$t = 80$	$t = 122$
LMP	$ 108 /MWh	$ 48 /MWh
Generation capacity of MG buses	588 kW	585 kW
Actual generation of MG buses	588 kW	583 kW
Demand of MG buses	900 kW	543 kW
Generation insufficiency	**312 kW**	---
Generation surplus	---	**40 kW**
Load shedding	8 kW	---
Load shed location	Bus 13	---

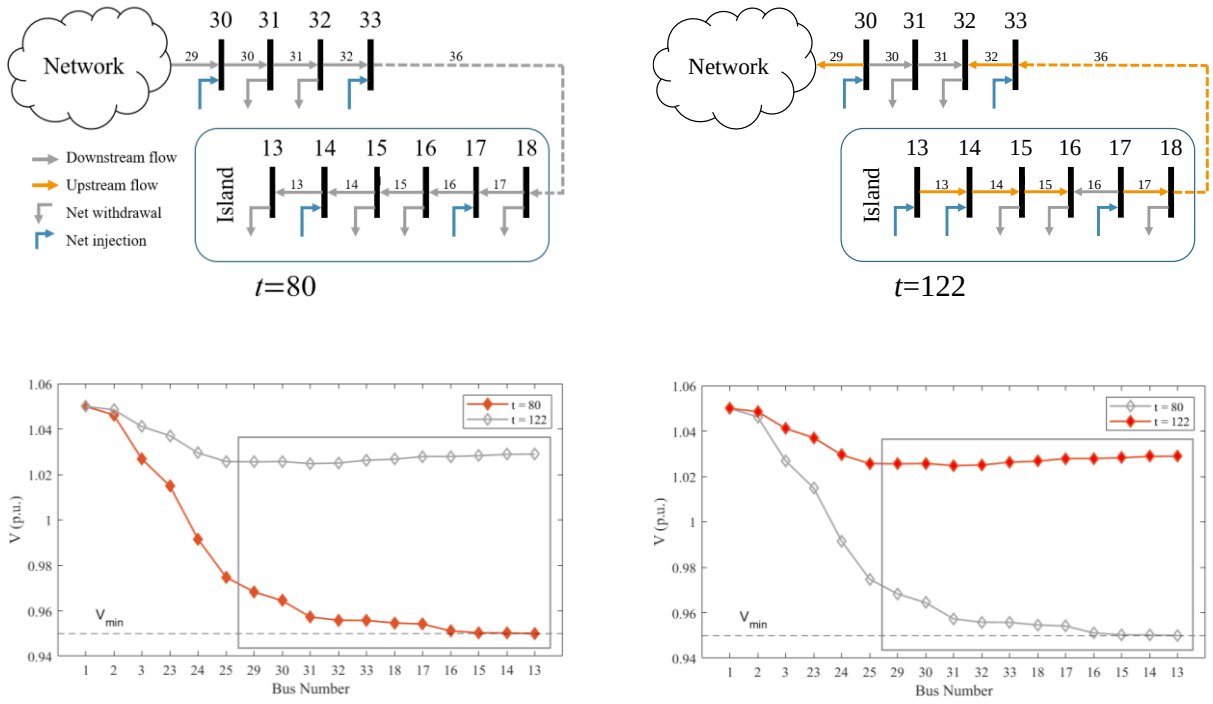

(a) (b)

Figure 16: Network flow directions at the end of the feeder, and voltage profile along the feeder for (a) the 80th hour (b) the 122nd hour.

local capacity and are injecting power into the medium-voltage network. Line flows are consistent with the radial topology established by the NR modeling approach. Bus 13—the furthest bus of this feeder—has a voltage of exactly 0.95 p.u., and thus its voltage constraint is active. Moreover, this means that load shedding is occurring within the island specifically to maintain voltage stability. Islanding within this hour would create the opportunity to define a new voltage reference (through the grid-forming inverter equipped at bus 17) that could circumvent the expensive load shedding associated with voltage management. However, the total load within the island exceeds the total generation capacity, so islanding would not actually avoid load shedding in this hour. For this reason, it is optimal for power to be *imported* into the island from the rest of the network.

Moving to $t = 122$, the relatively low system demand paired with an economic incentive to generate power from the DERs results in a high voltage profile across the feeder with no active voltage constraints. The total generation capability of the island for this hour is greater than the island's load, and the DERs at all sited buses have satisfied local demand and are injecting net power into the network. However, these injections are great enough at certain locations to *reverse* the direction of power flow upstream. If during this hour islanding were to be enforced, then some of the load being met by the island's cheap power would instead be met by drawing more power from the substation at the more expensive LMP. This of course is a suboptimal choice, so the optimal choice in this case is for power to be *exported* from the island to the rest of the network.

Based on these two cases, it seems that the combination of generation capacity, system load, and LMP affects whether importing or exporting power is optimal for a given hour. To avoid improper generalization, Figure 17 places the PCC line flows from the 80th and 122nd hour within the context of the entire testing period. From the figure it is clear that the island mainly imports power from the upstream network. This result is intuitive since it is less likely—given the full

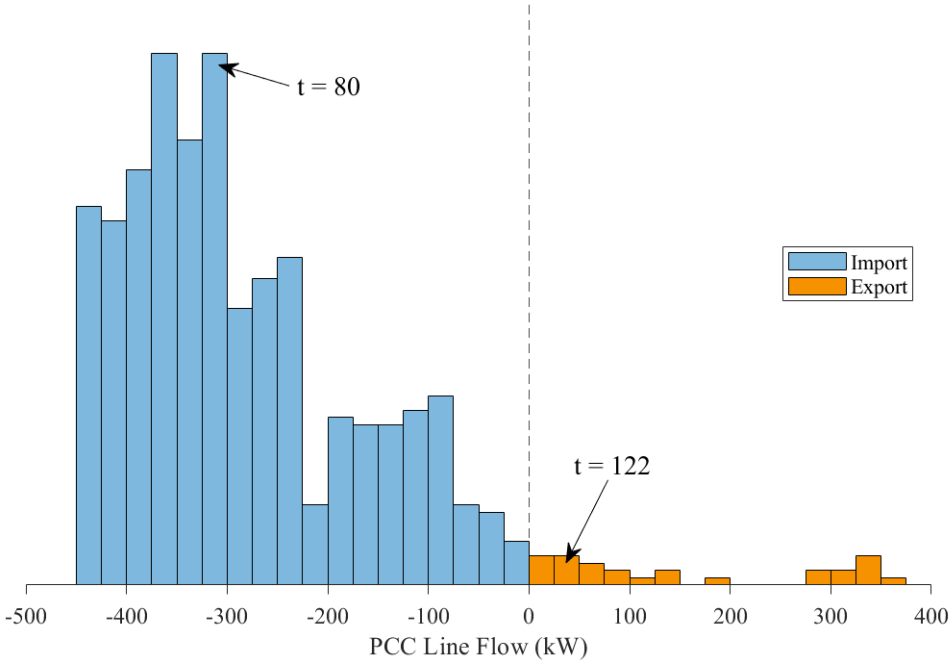

Figure 17: Histogram of line flows across the PCC line.

historical price curve—to obtain an instance where (1) the LMP is high enough to warrant running the CTs near full capacity and (2) the system load is low enough for the island to be able to export power. Although $t = 80$ is the time of highest system load, other hours of larger power export occur when power from the transmission network is cheap, so the CTs in the island remain idle. The hours of power export greater than $t = 122$ occur when more irradiance is available for the PVs to inject power at higher capacity.

Discussion

Based on the preceding case study, it can be concluded that microgrid islanding within the modeling framework proposed in this thesis results in one of three effects on the system. First, islanding allows for a new voltage reference to be formed, which can alleviate load shedding due to voltage management. Second, islanding can introduce or increase load shedding if done at a time where generation capacity cannot meet total demand, as with the $t = 80$ case. Third, and most interestingly, islanding can increase operational costs during times of net export, as cheaper power is curtailed and replaced by more expensive power from the connected transmission system, as with the $t = 122$ case.

The results of this thesis, then, suggest that microgrid islanding under non-emergency conditions (i.e. in the absence of one or more faults) does not provide economic benefit in terms of maximizing social welfare. However, the ability for a microgrid to island remains a powerful tool for increasing demand-side grid resiliency, and the work of this thesis suggests that this capability does not need to be directly incorporated into distribution system planning tools, as it would increase modeling complexity without providing direct or significant economic gains.

Bidirectional Power Flow in Radial Systems

As previously noted, the analysis of islanding performed in this case study reveals that the proposed DSP framework allowed for bidirectional power flow, which contributed to the suboptimality of islanding. Moreover, this conclusion offers broader insights to this field of research that warrant further discussion. Note that the DistFlow equations in [43] were originally developed in the context of reconfiguring *radial* networks for loss reduction and load balancing. This work considered passive flow, and its solution method involved iterations to solve due to limitations in computing at the time. In the decades that followed, the literature has adopted the DistFlow equations as common practice to model AC power flow for radial networks within a convex optimization framework, even though the systems being modeled have become increasingly *active* with the incorporation of various DERs. To the author's knowledge, the fact that bidirectional power flow is feasible within such a framework has been neither identified nor addressed despite many works that include DERs and NR within a radial topology. Bidirectional flows negate the original intention of radiality in distribution networks, which was to simplify the calculations of fault current directions and magnitudes for protective device (PD) settings [50]. Thus, solutions proposed by similar optimization frameworks will continue to diverge from the actual requirements of the systems being modeled as DERs continue to be integrated more and more into primary and secondary distribution networks.

As a way to move forward in addressing this issue, one could consider adding constraints that restrict reverse power flow. However, for DSP frameworks that include topology decisions, the sense of "normal" flow direction itself is dependent on binary decision variables. Any added constraints to flow direction in this case would likely introduce products of binaries, which, after appropriate reformulations, would result in an intractable number of binary variables relative to

network size. For this reason, the author suggests the need for a paradigm shift within distribution system modeling and optimization that will be delineated in Future Work.

CHAPTER 5
CONCLUSIONS AND FUTURE WORK

5.1 Conclusions

The past several decades have indicated the start of a revolution of the distribution network from passive and simple to active and complex. As generation technology evolves and expands, the need to adequately determine the right resource mix to meet future growth at least cost is becoming increasingly critical. In light of these facts, this thesis explores the intersections between the increasing affordability of DERs, the continued maturation of the microgrid concept, and the utility's role in adopting these technologies for greater economic efficiency and resiliency in the distribution system.

An optimization framework was developed to model the aforementioned interactions within the context of a traditional distribution system planning problem. Particular care was taken in the design of the planning model to develop a framework that co-optimizes as many interdependent decisions as possible while maintaining convexity for a global solution. The framework synthesizes a set of well-established convex modeling techniques to produce a MISOCP optimization framework that, most notably, models MVMG planning as a set of topology-based choices. This framework was then incorporated into a two-stage optimization algorithm introduced to model MVMG islanding capabilities on an hourly time scale. The result of the full planning model provides an optimal generation mix allocated from a provided budget, and an optimized network topology with a subset of the system converted to a set of microgrids capable of self-sustainment.

The developed DSP framework was tested on the IEEE 33-bus system as example of its capabilities to provide a system planner with a single, optimized solution. Moreover, economic analysis of utility microgrid investment was performed by comparing a baseline, one-area, and two-area case. The results from Case Study I (CS1) reveal that the incorporation of a multi-area approach to system planning can result in a solution that is more resilient to extreme price and load events, which are expected to occur with greater frequency in the future. CS1 also highlights the tradeoff between resiliency and cost depending on the assumed level of future risk.

In response to the results of CS1, a second case study (CS2) was conducted to investigate the economic drivers of microgrid islanding within the long-term horizon of system planning. The results refined and confirmed what was evidenced in CS1, namely that the ability to island does not present a specific economic advantage—within a radial distribution system and under normal operating conditions—even in the presence of load shedding. Further study of the results prompted a discussion on the presence of bidirectional flows when modeling AC radial systems with distributed generation, and a call to reconsider current modeling conventions as the ADN continues to become the new norm.

Application of the proposed DSP framework confirmed the feasibility to co-optimize DER investment and MVMG topology planning for utilities, and presents a promising first step to evaluate microgrid investment on solid economic grounds. Analysis of the case studies suggests that the MG islanding operation is most readily found to add value when considering emergency conditions and the unique revenue streams that result from them, such as serving unmet load immediately after one or more faults have been cleared.

5.2 Future Work

Ultimately, the work of this thesis was inspired by a desire to contribute to a more rapid adoption of clean, renewable energy facilitated by microgrids. The author sees several avenues through which future work can expand on the contributions presented here in order to progress toward an informed and efficient adoption of renewable technologies.

Testing of Developed Framework on Larger Systems

The most obvious suggestion for future work is to continue to investigate the potential of the proposed DSP framework by expanding the simulations in two ways. First, the planning model was developed to allow for an abstracted number of substation buses and desired MGs, so further testing could be conducting on the existing IEEE 33-bus system, e.g., for a three-area case to investigate whether the resulting interactions *between* the MGs allows for additional cost-saving opportunities.[4] Second, a larger test system could be introduced into the model and tested, preferably one that consists of multiple feeders connected through existing tie lines. In this way, the MGs resulting from the first stage of optimization could foreseeably be programmed in the second stage to allow for connection points to multiple feeders, allowing for more flexibility. However, this insight is not fully developed and would require care not to introduce overlapping binary logic.

[4] Solving Model (3.1) for three-area and four-area cases have already been verified by the author but not analyzed in detail.

Incorporation of Contingency Events in the Evaluation of Microgrid Planning

As previously mentioned, the literature has sufficiently demonstrated that microgrids can increase grid resiliency both in the presence of contingencies and after comprehensive blackouts, but little work has been done on evaluating these benefits relative to the cost of investment and the opportunity cost of other investment choices. This thesis focused on evaluation of utility microgrid investment under normal operating conditions; hence, a valuable opportunity remains to incorporate extreme conditions directly into the DSP problem. Since the start of this thesis, promising work has already emerged in the literature such as [51] and [52], both of which incorporate reliability metrics and post-fault response directly into a system planning horizon. Combining a similar approach with the multi-area optimization technique developed in this thesis could actualize a more holistic approach to utility microgrid planning.

Use of Meshed Distribution Networks When Incorporating DERs

As introduced in CS2, attempting to enforce unidirectional flow limits when modeling AC radial systems is computationally intractable and therefore an undesirable solution. Even if such constraints could be reasonably incorporated, they would ultimately limit the amount of renewable injections for the sake of antiquated protection schemes. Instead, it seems apparent that a better way forward is through a paradigm shift in the way that distribution system planning is approached in future research. Specifically, the inevitability of higher DER penetrations necessitates the widespread adoption of adaptive and differential protection schemes similar to that presented on the LVMG level in [50]. In order to support and accelerate this transition, future research should seek to adopt meshed test systems when performing optimization that includes DERs (which naturally cause bidirectional flows). In this way, more discoveries on the benefits of DERs and

MG interactions will have arisen by the time that smart protection equipment matures to facilitate this transition.

LIST OF REFERENCES

[1] "Combined Heat and Power Technology Fact Sheet Series." U.S. Department of Energy. https://www.energy.gov/sites/prod/files/2017/12/f46/CHP%20Overview-120817_compliant_0.pdf (accessed December 15, 2020.

[2] R. F. Fu, David; Margolis, Robert, "U.S. Solar Photovoltaic System Cost Benchmark Q1 2018," 03/15/2019 ed. National Renewable Energy Laboratory, 2019.

[3] W. J. Cole and A. Frazier, "Cost projections for utility-scale battery storage," National Renewable Energy Lab.(NREL), Golden, CO (United States), 2019.

[4] J. Cook *et al.*, "Quantifying the consensus on anthropogenic global warming in the scientific literature," *Environmental Research Letters*, vol. 8, no. 2, Apr-Jun 2013, Art no. 024024, doi: 10.1088/1748-9326/8/2/024024.

[5] "Rewable Power Generation Costs in 2019." [Online]. Available: https://www.irena.org/publications/2020/Jun/Renewable-Power-Costs-in-2019

[6] T. Yang, "10 - ICT technologies standards and protocols for active distribution network," in *Smart Power Distribution Systems*, Q. Yang, T. Yang, and W. Li Eds.: Academic Press, 2019, pp. 205-230.

[7] M. Milligan. (2015, November-December) Alternatives No More: Wind and Solar Power are Mainstays of a Clean, Reliable, Affordable Grid. *IEEE Power and Energy Magazine*. 78-87.

[8] M. B. J. von Appren, T. Stetz, K. Diwold, and D. Geibel. (2013, March-April) Time in the Sun: The Challenge of High PV Penetration in the German Electric Grid. *IEEE Power and Energy Magazine*. 78-87.

[9] S. Bahramirad, A. Khodaei, and R. Masiello, "Distribution Markets," *IEEE Power and Energy Magazine*, vol. 14, no. 2, pp. 102-106, 2016, doi: 10.1109/MPE.2016.2543121.

[10] B. Lasseter, "Microgrids [Distributed Power Generation]," *Proc. IEEE Power Engineer. Soc. Winter Meet.*, vol. 1, pp. 146-149, January 2001.

[11] D. E. Olivares *et al.*, "Trends in Microgrid Control," *IEEE Transactions on Smart Grid*, vol. 5, no. 4, pp. 1905-1919, 2014.

[12] W. El-Khattam, Y. Hegazy, and M. Salama, "An integrated distributed generation optimization model for distribution system planning," in *IEEE Power Engineering Society General Meeting, 2005*, 16-16 June 2005 2005, p. 2392 Vol. 3, doi: 10.1109/PES.2005.1489232. [Online]. Available: https://ieeexplore.ieee.org/document/1489232/

[13] H. A. Gil and G. Joos, "On the Quantification of the Network Capacity Deferral Value of Distributed Generation," *IEEE Transactions on Power Systems*, vol. 21, no. 4, pp. 1592-1599, 2006, doi: 10.1109/TPWRS.2006.881158.

[14] P. Paliwal, N. P. Patidar, and R. K. Nema, "A comprehensive survey of optimization techniques used for Distributed Generator siting and sizing," in *2012 Proceedings of IEEE Southeastcon*, 15-18 March 2012 2012, pp. 1-7, doi: 10.1109/SECon.2012.6196992.

[15] C. D. Rodríguez-Gallegos *et al.*, "A Siting and Sizing Optimization Approach for PV–Battery–Diesel Hybrid Systems," *IEEE Transactions on Industry Applications*, vol. 54, no. 3, pp. 2637-2645, 2018, doi: 10.1109/TIA.2017.2787680.

[16] O. D. M. Dominguez, M. P. Kasmaei, M. Lavorato, and J. R. S. Mantovani, "Optimal siting and sizing of renewable energy sources, storage devices, and reactive support devices to obtain a sustainable electrical distribution systems," *Energy Systems-Optimization Modeling Simulation and Economic Aspects*, vol. 9, no. 3, pp. 529-550, Aug 2018, doi: 10.1007/s12667-017-0254-8.

[17] Q. Li, R. Ayyanar, and V. Vittal, "Convex Optimization for DES Planning and Operation in Radial Distribution Systems With High Penetration of Photovoltaic Resources," *IEEE Transactions on Sustainable Energy*, vol. 7, no. 3, pp. 985-995, 2016, doi: 10.1109/tste.2015.2509648.

[18] B. Zou, J. Wang, and F. Wen, "Optimal investment strategies for distributed generation in distribution networks with real option analysis," *IET Generation, Transmission & Distribution*, vol. 11, no. 3, pp. 804-813, 2017, doi: 10.1049/iet-gtd.2016.0541.

[19] M. Kabirifar, M. Fotuhi-Firuzabad, M. Moeini-Aghtaie, and N. Pourghaderi, "Multistage Active Distribution Network Integrated Planning Incorporating Energy Storage Systems and Active Network Management," in *2020 IEEE 4th International Conference on Intelligent Energy and Power Systems (IEPS)*, 7-11 Sept. 2020 2020, pp. 163-168, doi: 10.1109/IEPS51250.2020.9263121.

[20] J. A. Taylor and F. S. Hover, "Convex Models of Distribution System Reconfiguration," *IEEE Transactions on Power Systems*, vol. 27, no. 3, pp. 1407-1413, 2012, doi: 10.1109/TPWRS.2012.2184307.

[21] R. A. Jabr, R. Singh, and B. C. Pal, "Minimum Loss Network Reconfiguration Using Mixed-Integer Convex Programming," *IEEE Transactions on Power Systems*, vol. 27, no. 2, pp. 1106-1115, 2012, doi: 10.1109/TPWRS.2011.2180406.

[22] S. Khodayifar, M. A. Raayatpanah, A. Rabiee, H. Rahimian, and P. M. Pardalos, "Optimal Long-Term Distributed Generation Planning and Reconfiguration of Distribution Systems: An Accelerating Benders' Decomposition Approach," *Journal of Optimization Theory and Applications*, vol. 179, no. 1, pp. 283-310, Oct 2018, doi: 10.1007/s10957-018-1367-5.

[23] L. Q. Bai, T. Jiang, F. X. Li, H. H. Chen, and X. Li, "Distributed energy storage planning in soft open point based active distribution networks incorporating network reconfiguration and DG reactive power capability," *Applied Energy*, vol. 210, pp. 1082-1091, Jan 2018, doi: 10.1016/j.apenergy.2017.07.004.

[24] Z. J. Wang, Y. Chen, S. W. Mei, S. W. Huang, and Y. Xu, "Optimal expansion planning of isolated microgrid with renewable energy resources and controllable loads," *Iet Renewable Power Generation*, vol. 11, no. 7, pp. 931-940, Jun 2017, doi: 10.1049/iet-rpg.2016.0661.

[25] L. Guo, W. J. Liu, B. Q. Jiao, B. W. Hong, and C. S. Wang, "Multi-objective stochastic optimal planning method for stand-alone microgrid system," *Iet Generation Transmission & Distribution*, vol. 8, no. 7, pp. 1263-1273, Jul 2014, doi: 10.1049/iet-gtd.2013.0541.

[26] G. P. Zhao and D. Wang, "Comprehensive Evaluation of AC/DC Hybrid Microgrid Planning Based on Analytic Hierarchy Process and Entropy Weight Method," *Applied Sciences-Basel*, vol. 9, no. 18, Sep 2019, Art no. 3843, doi: 10.3390/app9183843.

[27] Q. Peng, X. L. Wang, S. Shi, S. Wang, S. Yan, and Y. T. Chen, *Multi-objective Planning of Microgrid Considering Electric Vehicles Charging Load* (2020 5th Asia Conference on Power and Electrical Engineering). 2020, pp. 1172-1179.

[28] R. Morales, D. Saez, L. G. Marin, A. Nunez, and Ieee, "Microgrid Planning based on Fuzzy Interval Models of Renewable Resources," in *2016 Ieee International Conference on Fuzzy Systems*, (IEEE International Fuzzy Systems Conference Proceedings, 2016, pp. 336-343.

[29] H. Mehrjerdi, "Dynamic and multi-stage capacity expansion planning in microgrid integrated with electric vehicle charging station," *Journal of Energy Storage*, vol. 29, Jun 2020, Art no. 101351, doi: 10.1016/j.est.2020.101351.

[30] A. Khodaei, S. Bahramirad, and M. Shahidehpour, "Microgrid Planning Under Uncertainty," *IEEE Transactions on Power Systems*, vol. 30, no. 5, pp. 2417-2425, 2015, doi: 10.1109/TPWRS.2014.2361094.

[31] X. Guo, H. Guo, H. Z. Cheng, and Ieee, *Coordinated planning of distributed energy resources and microgrid network* (2016 Ieee/Pes Transmission and Distribution Conference and Exposition). 2016.

[32] T. J. Wang and X. H. Yang, "Optimal network planning of AC/DC hybrid microgrid based on clustering and multi-agent reinforcement learning," *Journal of Renewable and Sustainable Energy*, vol. 13, no. 2, Mar 2021, Art no. 025501, doi: 10.1063/5.0034816.

[33] M. Saleh, Y. Esa, N. Onuorah, and A. A. Mohamed, "Optimal microgrids placement in electric distribution systems using complex network framework," in *2017 IEEE 6th International Conference on Renewable Energy Research and Applications (ICRERA)*, 5-8 Nov. 2017 2017, pp. 1036-1040, doi: 10.1109/ICRERA.2017.8191215.

[34] M. I. Pathan, M. Al-Muhaini, and S. Z. Djokic, "Optimal reconfiguration and supply restoration of distribution networks with hybrid microgrids," *Electric Power Systems Research*, vol. 187, Oct 2020, Art no. 106458, doi: 10.1016/j.epsr.2020.106458.

[35] J. P. Zhu, Y. Yuan, and W. S. Wang, "An exact microgrid formation model for load restoration in resilient distribution system," *International Journal of Electrical Power & Energy Systems*, vol. 116, Mar 2020, Art no. 105568, doi: 10.1016/j.ijepes.2019.105568.

[36] T. Ding, Y. L. Lin, G. F. Li, and Z. H. Bie, "A New Model for Resilient Distribution Systems by Microgrids Formation," *Ieee Transactions on Power Systems*, vol. 32, no. 5, pp. 4145-4147, Sep 2017, doi: 10.1109/tpwrs.2017.2650779.

[37] C. Chen, J. H. Wang, F. Qiu, and D. B. Zhao, "Resilient Distribution System by Microgrids Formation After Natural Disasters," *Ieee Transactions on Smart Grid*, vol. 7, no. 2, pp. 958-966, Mar 2016, doi: 10.1109/tsg.2015.2429653.

[38] T. Ding, Y. L. Lin, Z. H. Bie, and C. Chen, "A resilient microgrid formation strategy for load restoration considering master-slave distributed generators and topology reconfiguration," *Applied Energy*, vol. 199, pp. 205-216, Aug 2017, doi: 10.1016/j.apenergy.2017.05.012.

[39] R. H. Kumar, N. Mayadevi, V. P. Mini, and S. Ushakumari, "Transforming distribution system into a sustainable isolated microgrid considering contingency," *Bulletin of the Polish Academy of Sciences-Technical Sciences*, vol. 67, no. 5, pp. 871-881, 2019, doi: 10.24425/bpasts.2019.130875.

[40] L. Che, X. P. Zhang, M. Shahidehpour, A. Alabdulwahab, and Y. Al-Turki, "Optimal Planning of Loop-Based Microgrid Topology," *Ieee Transactions on Smart Grid*, vol. 8, no. 4, pp. 1771-1781, Jul 2017, doi: 10.1109/tsg.2015.2508058.

[41] C. A. Cortes, S. F. Contreras, and M. Shahidehpour, "Microgrid Topology Planning for Enhancing the Reliability of Active Distribution Networks," *Ieee Transactions on Smart Grid*, vol. 9, no. 6, pp. 6369-6377, Nov 2018, doi: 10.1109/tsg.2017.2709699.

[42] N. Daryani, K. Zare, S. Tohidi, and J. M. Guerrero, "Dominated GSO algorithm for optimal microgrid construction to improve consumer side properties in a distribution system," *International Journal of Electrical Power & Energy Systems*, vol. 123, Dec 2020, Art no. 106232, doi: 10.1016/j.ijepes.2020.106232.

[43] M. E. Baran and F. F. Wu, "Network reconfiguration in distribution systems for loss reduction and load balancing," *IEEE Transactions on Power Delivery*, vol. 4, no. 2, pp. 1401-1407, 1989, doi: 10.1109/61.25627.

[44] P. Pareek and A. Verma, "Linear OPF with linearization of quadratic branch flow limits," in *2018 IEEMA Engineer Infinite Conference (eTechNxT)*, 13-14 March 2018 2018, pp. 1-6, doi: 10.1109/ETECHNXT.2018.8385365.

[45] T. Ding, K. Sun, C. Huang, Z. Bie, and F. Li, "Mixed-Integer Linear Programming-Based Splitting Strategies for Power System Islanding Operation Considering Network Connectivity," *IEEE Systems Journal*, vol. 12, no. 1, pp. 350-359, 2018, doi: 10.1109/JSYST.2015.2493880.

[46] Q. X. Shi *et al.*, "Network reconfiguration and distributed energy resource scheduling for improved distribution system resilience," *International Journal of Electrical Power & Energy Systems*, vol. 124, Jan 2021, Art no. 106355, doi: 10.1016/j.ijepes.2020.106355.

[47] S. Ma, L. Su, Z. Wang, F. Qiu, and G. Guo, "Resilience Enhancement of Distribution Grids Against Extreme Weather Events," *IEEE Transactions on Power Systems*, vol. 33, no. 5, pp. 4842-4853, 2018, doi: 10.1109/TPWRS.2018.2822295.

[48] S. Lei, C. Chen, Y. Song, and Y. Hou, "Radiality Constraints for Resilient Reconfiguration of Distribution Systems: Formulation and Application to Microgrid Formation," *IEEE Transactions on Smart Grid*, vol. 11, no. 5, pp. 3944-3956, 2020, doi: 10.1109/TSG.2020.2985087.

[49] "Public Data - Data Miner 2." PJM. https://dataminer2.pjm.com/list (accessed January 19, 2021.

[50] L. Che, M. E. Khodayar, and M. Shahidehpour, "Adaptive Protection System for Microgrids: Protection practices of a functional microgrid system," *IEEE Electrification Magazine*, vol. 2, no. 1, pp. 66-80, 2014, doi: 10.1109/MELE.2013.2297031.

[51] Q. Shi *et al.*, "Resilience-Oriented DG Siting and Sizing considering Stochastic Scenario Reduction," *IEEE Transactions on Power Systems*, pp. 1-1, 2020, doi: 10.1109/TPWRS.2020.3043874.

[52] Z. Li, W. Wu, X. Tai, and B. Zhang, "A Reliability-Constrained Expansion Planning Model for Mesh Distribution Networks," *IEEE Transactions on Power Systems*, vol. 36, no. 2, pp. 948-960, 2021, doi: 10.1109/TPWRS.2020.3015061.

APPENDIX

Table 6: Appendix – IEEE 33-Bus System per-unit bases

Parameter	Value
V_{BASE} (kV)	12.66
S_{BASE} (MVA)	10.0
Z_{BASE} (Ohm)	16.028

Table 7: Appendix – IEEE 33-Bus System load data

Bus	Real Demand (kW)	Reactive Demand (kW)	Nominal Voltage (kV)
1	0	0	12.66
2	100	60	12.66
3	90	40	12.66
4	120	80	12.66
5	60	30	12.66
6	60	20	12.66
7	200	100	12.66
8	200	100	12.66
9	60	20	12.66
10	60	20	12.66
11	45	30	12.66
12	60	35	12.66
13	60	35	12.66
14	120	80	12.66
15	60	10	12.66
16	60	20	12.66
17	60	20	12.66
18	90	40	12.66
19	90	40	12.66
20	90	40	12.66
21	90	40	12.66
22	90	40	12.66
23	90	50	12.66
24	420	200	12.66
25	420	200	12.66
26	60	25	12.66
27	60	25	12.66
28	60	20	12.66
29	120	70	12.66
30	200	600	12.66
31	150	70	12.66
32	210	100	12.66
33	60	40	12.66

Table 8: Appendix – IEEE 33-Bus System branch data

Line	From Bus	To Bus	R (p.u.)	X (p.u.)
1	1	2	0.0058	0.0029
2	2	3	0.0308	0.0157
3	3	4	0.0228	0.0116
4	4	5	0.0238	0.0121
5	5	6	0.0511	0.0441
6	6	7	0.0117	0.0386
7	7	8	0.0444	0.0147
8	8	9	0.0643	0.0462
9	9	10	0.0651	0.0462
10	10	11	0.0123	0.0041
11	11	12	0.0234	0.0077
12	12	13	0.0916	0.0721
13	13	14	0.0338	0.0445
14	14	15	0.0369	0.0328
15	15	16	0.0466	0.0340
16	16	17	0.0804	0.1074
17	17	18	0.0457	0.0358
18	2	19	0.0102	0.0098
19	19	20	0.0939	0.0846
20	20	21	0.0255	0.0298
21	21	22	0.0442	0.0585
22	3	23	0.0282	0.0192
23	23	24	0.0560	0.0442
24	24	25	0.0559	0.0437
25	6	26	0.0127	0.0065
26	26	27	0.0177	0.0090
27	27	28	0.0661	0.0583
28	28	29	0.0502	0.0437
29	29	30	0.0317	0.0161
30	30	31	0.0608	0.0601
31	31	32	0.0194	0.0226
32	32	33	0.0213	0.0331
33	21	8	0.1248	0.1248
34	9	15	0.1248	0.1248
35	12	22	0.1248	0.1248
36	18	33	0.0312	0.0312
37	25	29	0.0312	0.0312

VITA

Ian Schomer was born and raised in Knoxville, Tennessee. He graduated from Maryville College with a B.S. in Mathematics in the Spring of 2019. Ian continued his education by enrolling at the University of Tennessee, Knoxville in the Fall of 2019 to pursue a M.S. degree in Electrical Engineering with a concentration in Power Systems. He graduated the program in the Summer of 2021. During his graduate study, Ian was a research assistant in the Power and Energy Systems group at Oak Ridge National Laboratory, and an Energy Analyst intern at Newton Energy Group (NEG). He plans to move to Seattle, Washington after the completion of his degree to begin his career at NEG as an Energy Analyst.